

SECTION III

HYDRATE DISSOCIATION MODELLING AND IMPLICATIONS OF HYDRATE DISSOCIATION DURING DRILLING IN ARCTIC OFFSHORE AND ONSHORE ENVIRONMENTS

Prepared By

**V.A. Kamath
S.P. Godbole**

TABLE OF CONTENTS FOR SECTION III

<u>Sub- Section</u>	<u>Title</u>	<u>Page No.</u>
1.0	Implications of Dissociation of In-Situ Gas Hydrate Deposits.....	1
1.1	Introduction.....	1
1.2	Drilling Problems.....	1
1.3	Production of Natural Gas From Hydrates.....	3
1.4	References.....	6
2.0	Mathematical Model For Drilling in the Presence of Hydrates.....	8
2.1	Introduction.....	8
2.2	Model Considerations and Assumptions.....	8
2.3	Model Equations.....	11
2.4	Fundamental Hydrate Dissociation Model.....	20
2.4.1	Dimensionless Variables.....	20
2.4.2	Dimensionless Differential Equations and Boundary Conditions.....	23
2.4.3	General Solution Method of the Fundamental Hydrate Dissociation Model.....	26
2.4.4	Gas Influx Calculations.....	28
2.5	Summary and Conclusions.....	29
2.6	Nomenclature.....	30
2.7	References.....	34
2.8	Appendix.....	35
A.	Determination of Convective Heat Transfer Coefficients.....	35
B.	Determination of Energy Source Terms.....	36

3.0 Development of Guidelines for Drilling in the Presence of Hydrates.....	37
3.1 Hydrate Stability Zones.....	37
3.2 Reservoir Parametric Study.....	38
3.2.1 Geothermal Conditions.....	41
3.2.2 Hydrate Zone Depth.....	41
3.2.3 Hydrate Zone Thickness.....	41
3.2.4 Porosity.....	43
3.2.5 Drilling Parameter Analysis.....	43
3.2.6 Wellbore Radius.....	46
3.2.7 Pressure.....	50
3.2.8 Temperature.....	52
3.3 Selection of Parameters.....	58
3.4. References.....	62

1.0 IMPLICATIONS OF DISSOCIATION OF IN-SITU GAS HYDRATE DEPOSITS

1.1 Introduction

The presence of natural gas hydrates in arctic and subsea regions is well documented. Hydrate cores have been obtained from the Gulf of Mexico, the western coast of Guatemala, and in 1972, ARCO and EXXON recovered a hydrate core sample near Prudhoe Bay, Alaska. In addition, hydrate deposits in the Canadian and Russian Arctic are known to exist (Bily and Dick, 1974; Makogon, 1965).

Gas hydrates are crystalline compounds (clathrates) of gas and water, which are formed at relatively low temperatures and high pressures. These hydrates occupy much less volume than the unhydrated natural gas and water. One hundred percent methane saturated hydrates can contain up to 181.3 standard cubic feet of methane in hydrated form in just one cubic foot of pure hydrate. It is because of this concentrated form that natural gas hydrates have generated such interest as a potential future energy source, and that precautions must be taken when drilling through hydrate bearing formations.

1.2 Drilling Problems

Drilling through hydrate formation can cause well control problems due to severe mud gasifications if proper drilling procedures are not followed. Sizeable gas kicks and potential blowout conditions have been reported in the literature (Davidson et al, 1978; Franklin, 1979). Problems of well control due to severe mud gasification were reported by Imperial Oil Ltd. (Bily

and Dick, 1974), and Panarctic Oils Ltd. (Franklin, 1979). Other hydrate experiences include fizzed drill cuttings and wellbore freeze-up and casing collapse (Makogon, 1965; Franklin, 1979).

During drilling through a naturally occurring hydrate zone, hydrates are exposed to an increased temperature which causes dissociation of hydrates into gas and water, providing gas influx into the wellbore. This gas reduces the hydrostatic pressure of the mud column, further accelerating the hydrate dissociation in the vicinity of the wellbore. If the dissociation is rapid and significant, it can introduce a large gas influx from the dissociated hydrate zone into the wellbore causing a gas kick. The gas kick control problem has been discussed by Nickens (1985) and Ekrann and Rommetveit (1985).

Several specific examples of drilling problems encountered while drilling through hydrate zones have been discussed by Franklin (1979). The two most notable examples he reports are for wells drilled at Mearne Point on Mellville Island and in Jackson Bay. Problems encountered in the Mearne Point well included: a 22 percent gas cut at 356 meters (1,168 ft.); drill stem tools became frozen in the hole at the same depth; a sizeable gas kick occurred at 895 meters (2,936 ft.); hole stability problems were encountered at a depth of 1,676 meters (5,499 ft.); and while logging at a depth of 1,676 meters, a gas kick occurred and the logging tools were lost down the hole.

Incidents reported at the Jackson Bay well were just as significant. A 50 barrel kick was taken at a depth of 1,715 feet. Gas flow after each connection to a depth of 4,000 feet

resulted in the loss of about 5 barrels of mud per connection. At a depth of 4,000 feet, three days of circulation with increased mud density (14 lb/gal) were required to sufficiently stabilize the hole for the running of casing. In drilling below this depth, a background gas cut of 1 to 5 percent was noted while drilling, and a gas cut of 10 to 12 percent was recorded on connections.

Currently, two different methods are used to drill through hydrate containing formations. Predominately, cool drilling fluid with higher mud weight at high circulation rates is used to slow or prevent hydrate dissociation in the formation. Panarctic Oils Ltd., alternatively, tried to promote the dissociation at early times while the drill pipe is in the hole by using low weight muds with proper degassing equipment at the surface (Franklin, 1980).

1.3 Production of Natural Gas From Hydrates

The amount of natural gas bound in hydrate form has been estimated to be in excess of 10^{20} standard cubic feet, an overwhelming quantity when you consider the world's conventional gas resources are estimated to be 2.9×10^{15} standard cubic feet. Because the solid hydrates are immobile and relatively impermeable, they need to be dissociated into gas and water in order to produce natural gas from the reservoir in a conventional gas well.

The stability of natural gas hydrates is a function of three variables, namely pressure, temperature, and reservoir brine

salinity. Dissociating hydrates into gas and water required that one of these three parameters be altered in such a fashion as to destabilize the hydrates. There have been several methods suggested in the literature (McGuire, 1981; Holder et al, 1982; Holder and Angert, 1982; Bayles et al, 1984; Kamath and Godbole, 1985; Selim and Sloan, 1985). These include thermal recovery techniques such as steam injection or stimulation, hot water injection and fire flooding, depressurization, and injection of chemicals such as methanol or glycol which cause hydrate destabilization.

Holder et al (1982) showed that thermal recovery techniques are energy efficient from a thermodynamic standpoint, i.e., the heat required to dissociate hydrates is only a small fraction (about one tenth) of the heat that is obtained by burning the gas produced from the hydrates. Of the thermal recovery methods suggested, each has its own merits and demerits. In steam injection and fire flooding, heat losses could be severe for thin hydrate zones, but could be thermally efficient for thicker zones (greater than 50 feet). Fire flooding could cause dilution of the gas produced and thereby reduce its energy value. Hot water injection will yield lower heat losses, but injectivity of water into the hydrate reservoir will govern the applicability of the method. The injection water temperature should be low enough to avoid excessive heat losses, yet high enough to avoid unrealistically high injection rates. Hydraulic fracturing could be employed to improve water injectivity, but could result in lower heat transfer efficiencies due to channeling effects.

In 1984, Bayles et al presented a steam cycling model gas production from a hydrate reservoir. They found gas production to vary from 2.5 to 110 million standard cubic feet per year for a variety of reservoirs. The energy efficiency ranged from a low of 4.0 to a high of 9.6 combustible energy of the produced gas to the energy of the injected steam.

Selim and Sloan (1985) presented a model for dissociation of pure hydrates and found the energy efficiency to be 13, which is close to the thermodynamic efficiency. This should have been expected since their model does not consider heat losses or a porous rock matrix structure containing the hydrates.

Also in 1985, Kamath and Godbole presented a hot brine stimulation model for gas production from natural gas hydrates. For a 100 foot thick hydrate reservoir, they found an overall energy efficiency ratio of approximately 9 to 13 after 1,000 days for various brine salinities. Their study also concluded that brine injection resulted in higher thermal efficiencies and therefore higher gas production than steam for the same heat injection rate. This conclusion is, however, based on the assumption that the dissociated zone volume was capable of handling the predetermined injection rate of hot water.

Holder and Angert (1982) studied the depressurization scheme of dissociating hydrates. In this method, the sensible heat of the reservoir provides the energy necessary for hydrate dissociation. In this method, the gas pressure adjacent to the solid hydrate must be reduced. The hydrates, which produce their own vapor pressure, will dissociate until their vapor pressure is

reattained. In doing this, the hydrates exhibit a Joule-Thompson effect, becoming colder as they dissociate. A temperature gradient is thus generated between the hydrates and the surrounding formation and heat must flow to the hydrates. By keeping the pressure low by removing gas, the hydrates continue to dissociate, remaining colder than the surrounding media, thus maintaining the temperature gradient and heat flux to the hydrates. In their study, a hydrate layer was assumed to exist in association with a conventional gas layer. They found that the hydrates may account for up to 30 percent of the total gas production under this scheme.

Use of hydrate inhibitors such as methanol or glycol has not been studied in detail, but it may be safe to assume that their use would be governed by economics since large quantities of these relatively expensive chemicals may be required to ensure sufficient gas production.

1.4 References

- Bayles, G.A., Sawyer, W.K., Anada, H.R., Reddy, S. and Malone, R.D.: "A Steam Cycling Model for Gas Production From a Hydrate Reservoirs", Paper presented at the American Institute of Chemical Engineers Winter National Meeting, March 11-14, 1984 held in Atlanta, GA.
- Bily, C. and Dick, J.W.L.: "Naturally Occuring Gas Hydrates in the Mackenzie Delta, N.W.T." Bulletin of Canadian Petroleum Geologists, Vol. 22, No. 3 (1974).
- Davidson, D.W., El-Defrawy, M.K., Fuglem, M.O., and Judge, A.S.: "Natural Gas Hydrates in Northern Canada", The National Research Council of Canada, Proceedings of the Third International Conference on Permafrost, July 10-14, Vol. 1, pp 937-943, 1978.
- Ekrann, S., and Rommelveld, R.: "A Simulator for Gas Kicks in Oil Based Drilling Muds", Paper presented at the 60th Annual

Technical Conference and Exhibition of the SPE, held in Las Vegas, Nevada, SPE Paper #16182 (Sept. 1985).

Franklin, L.J.: "Hydrates in the Arctic Islands", Article 5, Proceedings of Workshop on Clathrates (Gas Hydrates) in the National Petroleum Reserve in Alaska, July 16-17, Menlo Park, CA, Edited by A.L. Bowher (1979).

Franklin, L.J.: "In-Situ Hydrates -- A Potential Gas Resource", Petroleum Engineers International, pp. 112-122 (Nov. 1980).

Holder, G.D. and Angert, P.F.: "Simulation of Gas Production from a Reservoir Containing Both Gas Hydrates and Free Natural Gas", SPE Paper 11105, presented at the 57th Annual Fall Technical Conference and Exhibition of the Society of Petroleum Engineers of AIME held in New Orleans, LA, Sept. 26-29, 1982.

Holder, G.D., Angert, P.F., John, V.T. and Yen, S.: "A Thermodynamic Evaluation of Thermal Recovery of Gas from Hydrates in the Earth", J. Pet. Tech., p. 1122, May 1982.

Kamath, V.A. and Godbole, S.P.: "Evaluation of Hot Brine Stimulation Technique for Gas Production From Natural Gas Hydrates", SPE Paper 13596, presented at the SPE 1985 California Regional Meeting, held in Bakersfield, CA, March 27-29, 1985.

Kvenvolden, K.A. and McMenamin, M.A.: "Hydrates of Natural Gas: A Review of Their Geologic Occurance", U.S. Geol. Sur. Circ., 1980.

Makogon, Y.F.: "Hydrate Formation in Gas Bearing Strata Under Permafrost", Gouzou, Promst., Vol. 5 (1965).

Mathews, M.: "Logging Characteristics of Methane Hydrates", The Log Analyst, pp. 26-63k (May-June 1986).

McGuire, P.L.: "Methane Gas Production by Thermal Stimulation", paper presented at the Fourth Canadian Permafrost Conference, Calgary, Alberta, March 2-6, 1981.

Nickens, H.N.: "A Dynamic Computer Model of a Kicking Well: Part I - The Theoretical Model, Part II - Model Predictions and Conclusions", Paper Presented at the 60th Annual Technical Conference and Exhibition of the SPE, held in Las Vegas, Nevada, SPE Paper #16183, 16186 (Sept. 1985).

Selim, M.S. and Sloan, E.D.: "Modeling of the Dissociation of an In-Situ Hydrate", SPE Paper 13597, presented at the SPE 1985 California Regional Meeting, held in Bakersfield, CA, March 27-29, 1985.

2.0 MATHEMATICAL MODEL FOR DRILLING IN THE PRESENCE OF HYDRATES

2.1 Introduction

The two-dimensional transient heat transfer model developed in this study couples the hydraulics and heat transfer in the wellbore with hydrate dissociation (and/or permafrost thaw) for both arctic and subsea locations. This model was derived from the wellbore heat transfer models of Keller et al (1973) and Marshall and Bentsen (1982) and the development of a fundamental hydrate dissociation model.

2.1 Model Considerations and Assumptions

Figure 1 represents the physical model on which the computer model is based for arctic regions. The model includes options for a full well completion scheme with any number of casing strings, or a simplified version which neglects the well completion and assumes a uniform hydraulic radius. For subsea locations, an option is included which either allows or neglects a riser casing to the platform.

The assumptions incorporated in this model for the drilling fluid and wellbore region include:

1. Heat transfer within the drilling fluid is by axial convection. Conduction is negligible except when circulation is stopped.

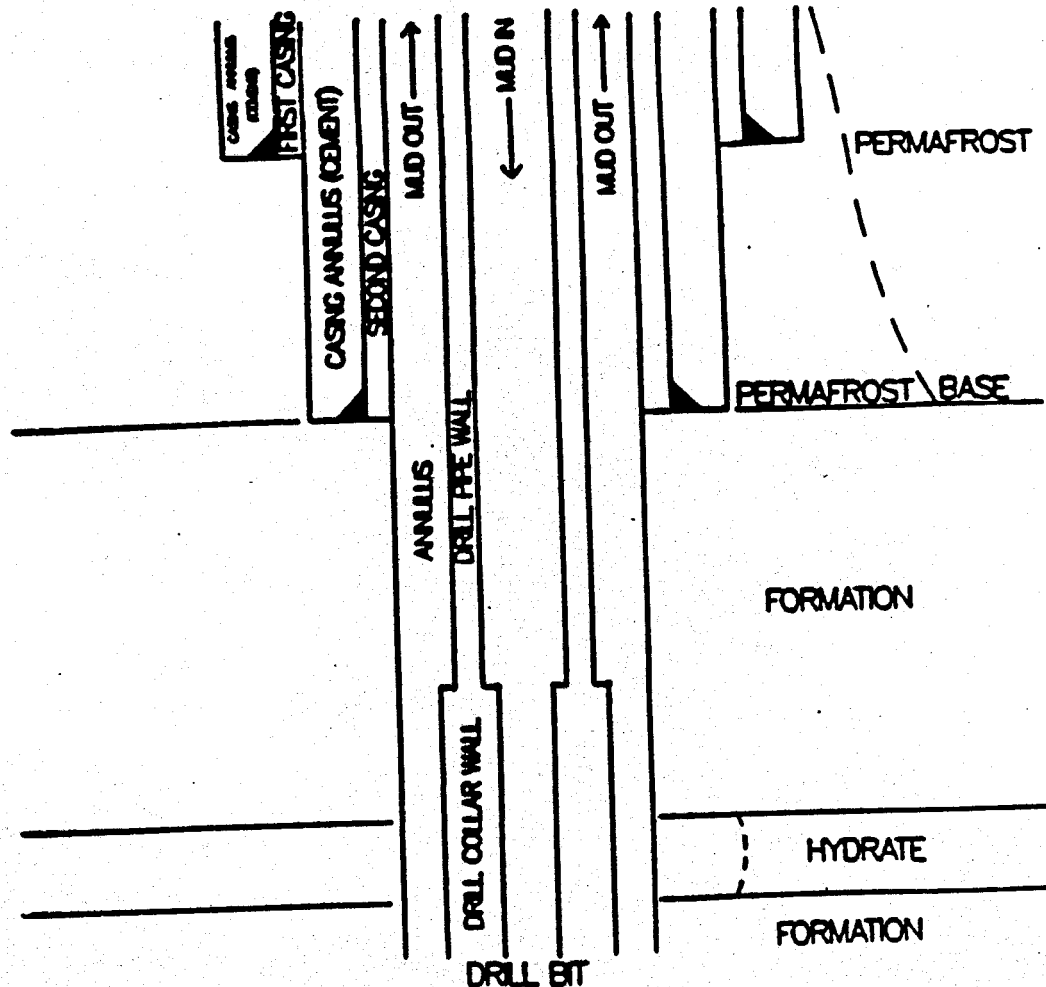


Figure 1: Schematic Diagram of a Well for the Arctic Region

2. Radial temperature gradients within the drilling fluid are negligible.
3. Radial conduction in the drill pipe wall is negligible compared to the radial convection between the drilling fluid and pipe wall.
4. Heat generation by viscous dissipation within the drilling fluid is negligible.
5. Fluid properties, i.e. density, thermal conductivity, and heat capacity, are independent of temperature.

Within the formation, there are five distinct zones that need to be accounted for: thawed permafrost region, unthawed permafrost region, solid formation, dissociated hydrate region, and solid hydrate region. The assumptions incorporated into the model for these five zones include:

6. Effects beyond the outer boundaries of the system are negligible.
7. There are no heat sources or sinks.
8. Each zone is individually homogeneous and isotropic.
9. Heat transfer in each region is by conduction only.
10. The thermophysical properties of each zone, i.e. thermal conductivity, heat capacity, and density, are constant within each zone and different across the boundaries separating each zone.
11. The formation above and below the hydrate zone is impermeable.
12. The gas produced from the dissociation of hydrates migrates rapidly to the well.

13. The hydrate zone is completely saturated with methane hydrates.

2.3 Model Equations

Five partial differential equations may be written to describe energy balances within the system. The heat flow within the drill string is described by Equation (1).

$$8.021 \rho_m C_p m q_m \frac{\partial T_p}{\partial z} + 2\pi r_{pi} h_{pi} (T_{pi} - T_w) \\ = - \rho_m C_p m \pi r_{pi}^2 \frac{\partial T_p}{\partial t} + Q_{pi} \quad (1)$$

The terms on the left represent the vertical and radial heat convection, respectively. The energy accumulation and source terms are represented by the right side terms, respectively.

Equation (2) represents the energy balance in the drill pipe wall.

$$k_w \frac{\partial^2 T_w}{\partial z^2} + \frac{2r_{pi} h_{pi}}{(r_{po}^2 - r_{pi}^2)} (T_{pi} - T_w) \\ + \frac{2r_{po} h_{po}}{(r_{po}^2 - r_{pi}^2)} (T_a - T_w) \\ = \rho_w C_p w \frac{\partial T_w}{\partial t} \quad (2)$$

The right-hand term is the heat accumulation within the wall. The left side terms represent, respectively, vertical heat

conduction within the wall, radial heat transfer to (from) the pipe wall from (to) the fluid inside the drill pipe, and radial heat transfer from (to) the pipe wall to (from) the annulus fluid.

The energy balance in the flow annulus is given by Equation (3).

$$\begin{aligned}
 & 8.021 \rho_{\text{meq}} C_{\text{p,meq}} q_m \frac{\partial T_a}{\partial z} + 2\pi r_{po} h_{po} (T_w - T_a) \\
 & + \rho \pi r_{wb} h_{wb} (T_k - T_a) \\
 & = \rho_{\text{meq}} C_{\text{p,meq}} (r_{wb}^2 - r_{po}^2) \frac{\partial T_a}{\partial t} - Q_a,
 \end{aligned} \tag{3}$$

$k = c, \text{ for, } D_p, \text{ DH}$

The left-hand terms include the vertical heat convection within the fluid, radial convection between the pipe wall and annulus fluid, and radial convection between the annulus fluid and the formation (or casing). On the right-hand side are the energy accumulation term and the energy source term, respectively.

Equation (4) expresses the energy balance in the first grid inside the formation or casing.

$$\begin{aligned}
 & \frac{\partial^2 T_k}{\partial z^2} + \frac{1}{r} \frac{\partial T_k}{\partial r} + \frac{\partial^2 T_k}{\partial r^2} \\
 & + \frac{2r_{wb} h_{wb} (T_a - T_k)}{k_k \left[\left(\frac{r_i + r_o}{2} \right) - r_{wb}^2 \right]} \quad (4)
 \end{aligned}$$

$$= \frac{1}{\alpha_k} \frac{\partial T_k}{\partial t}, k = c, \text{for, } D_p, D_h$$

The left-hand terms are the vertical and radial conduction terms and the radial convection between the annulus fluid and the formation, respectively. The energy accumulation term appears on the right-hand side. The subscript on the thermophysical properties indicates that this equation, depending on the completion scheme and depth location, may be applied to four different materials or zones, i.e., casing, thawed permafrost, solid formation, or dissociated hydrate region.

The final equation represents the energy balance elsewhere within the completion scheme or formation.

$$\frac{\partial^2 T}{\partial z^2} + \frac{1}{r} \frac{\partial T}{\partial r} + \frac{\partial^2 T}{\partial r^2} = \frac{1}{\alpha_k} \frac{\partial T}{\partial t}, \quad (5)$$

$$k = c, c_e, D_p, S_p, \text{for, } D_h, S_h$$

This equation is the well known two-dimensional cylindrical coordinate heat conduction equation. The subscript on the thermal diffusivity indicates that this equation may be applied to seven different materials, i.e., casing, casing annular material (cement), thawed permafrost, unthawed permafrost, solid formation, dissociated hydrate region, and solid hydrate regions.

In order to solve these equations we need the boundary conditions, the wellbore hydraulics, a means of determining the convective heat transfer coefficients for the particular fluid

rheology and flow regime, i.e. turbulent or laminar, and the energy source terms within the wellbore region. Due to the limited space available, the wellbore hydraulics will not be presented here, but rather, referenced as being the same as presented in Bourgoyn et al (1986) for Newtonian fluids, Bingham plastics, and power law fluids. The correlations for determining the convective heat transfer coefficients and the method of evaluating the energy source terms are presented in Appendix A.

The appropriate initial and boundary conditions are described below. The initial condition describes the initial temperature profile as being the geothermal gradient:

$$T_{i,j}^0 = T_{ms} + g_G z_j \quad (6)$$

The upper and lower boundary conditions are respectively:

$$\frac{\partial T}{\partial z} = 0, z = 0 \quad (7)$$

$$T_{i,j_{max}+1}^n = T_{i,j_{max}+1}^0 \quad (8)$$

The inner and outer radial boundary conditions indicate no heat flow across these boundaries:

$$\frac{\partial T}{\partial r} = 0, r = 0 \quad (9)$$

$$\frac{\partial T}{\partial r} = 0, r = r_e \quad (10)$$

The innermost upper grid temperature is defined as the fluid inlet temperature:

$$T_{1,0}^n = T_{mi} \quad (11)$$

Equation (12) expresses the requirement that the temperatures be equal at the drill bit depth within the wellbore:

$$T_{1,jmax}^n = T_{2,jmax}^n = T_{3,jmax}^n \quad (12)$$

Because thawing of permafrost and dissociation of hydrates represent moving boundary problems, boundary conditions at the moving boundaries separating the thawed and unthawed permafrost regions and the dissociated and undisassociated hydrate regions are required. These boundary conditions are of the same form for either permafrost or hydrates and so indicated by subscripts for each region. For the permafrost region, the first moving boundary condition expresses the requirement that the boundary be an isotherm:

$$T_{Dp}(r_{fp}, z_{fp}, t) = T_{Sp}(r_{fp}, z_{fp}, t) = T_{fp} \quad (13)$$

This is not true for the hydrate moving boundary as it is a strong function of pressure and therefore vertical position:

$$T_{DH}(r_{fH}, z_{fH}, t) = T_{SH}(r_{fH}, z_{fH}, t) = T_{fH}(z_{fH}) \quad (14)$$

The second set of moving boundary conditions are identical in form and express the requirement that the heat flux entering the boundary less the heat flux leaving the boundary be equal to the amount of permafrost thawed or hydrate dissociated:

$$\left\{ 1 + \left[\frac{\partial s(z,t)}{\partial z} \right]^2 \right\} [k_{Sk} \frac{\partial T_{Sk}(r,z,t)}{\partial r} - k_{Dk} \frac{\partial T_{Dk}(r,z,t)}{\partial r}] = -\rho_k L_{fk}(z) \frac{\partial r_{fk}}{\partial t}, \quad (15)$$

$k = p, H$

$$\left\{ 1 + \left[\frac{\partial s(r,t)}{\partial r} \right]^2 \right\} [k_{Sk} \frac{\partial T_{Sk}(r,z,t)}{\partial z} - k_{Dk} \frac{\partial T_{Dk}(r,z,t)}{\partial z}] = -\rho_k L_{fk}(z) \frac{\partial z_{fk}}{\partial t}, \quad k = p, H \quad (16)$$

Equations (15) and (16) express the rate of front advance in the radial and vertical directions, respectively.

The data utilized in this study are included in Tables 1 and 3.

The partial differential equations are written in a fully implicit finite difference form and the temperature distributions are solved by a direct solution method involving the LU decomposition approach. The solution of the wellbore hydraulics and heat transfer model indicated that the thermal gradient in the vertical direction in the wellbore for the thickness of the hydrate zone is not significant. Therefore, we assumed a constant temperature front in the wellbore and analyzed the decoupled hydrate dissociate model. The dimensionless form of fundamental hydrate dissociation model is discussed in detail.

TABLE 1
Wellbore, Drilling Fluid and Reservoir Parameters

ρ_{for}	= 167 (lb/ft ³)
Cp_{for}	= .2 (Btu/lb °F)
k_{for}	= 1.36 (Btu/hr ft °F)
ρ_{wat}	= 62.4 (lb/ft ³)
Cp_{wat}	= 1.08 (Btu/lb °F)
k_{wat}	= 0.343 (Btu/hr ft °F)
Cp_{C1}	= 0.5 (Btu/lb °F)
k_{C1}	= 0.0178 (Btu/ft hr °F)
ρ_h	= 57.1 (lb/ft ³)
Cp_h	= 0.54 (Btu/lb °F)
k_h	= 0.2274 (Btu/lb °F)
β_h	= 181.3 (SCF/ft ³ hydrate)
S_h	= 1.0
S_g	= 0.2
S_{wat}	= 0.8
r_e	= 0.8
A_{bit}	= 0.451 (ft ²)
k_m	= 1.0 (Btu/ft hr °F)
Cp_m	= 0.4 (Btu/lb °F)
ρ_w	= 486.0 (lb/ft ³)
k_w	= 25.28 (Btu/ft hr °F)

TABLE 2
Key Process Parameters

<u>Parameter</u>	<u>Range</u>
Wellbore Diameter, D_{wb}	6-12 (inches)
Hydrate Zone Thickness, H_{Hyd}	20-150 (feet)
Mud Density, ρ_m	10-18 (lb/gal)
Mud Viscosity, μ_m	20-100 (cp)
Mud Circulation Rate, q_m	100-500 (gal/min)
Bottom-Hole Mud Temperature, T_m	40-120 ($^{\circ}\text{F}$)
Geothermal Gradient, g_G	0.01-0.05 ($^{\circ}\text{F}/\text{ft}$)
Sea Depth, z_{sea}	1,000-8,000 (ft)
Mud Inlet Temperature, T_{mi}	50-120 ($^{\circ}\text{F}$)

TABLE 3

Base Case Model Parameters

D_{pi}	= 5.921 (in)
D_{po}	= 6.625 (in)
D_{wb}	= 8.375 (in)
ρ_m	= 10.0 (lb/gal)
μ_m	= 45.0 (cp)
q_m	= 200 (gal/min)
ϕ	= 0.2
H_{Hyd}	= 20 (ft)
z_{Hyd}	= 3,500 (ft)
z_{prb}	= 2,500 (ft)
g_G	= 0.01 ($^{\circ}\text{F}/\text{ft}$)
T_{ms}	= 10 ($^{\circ}\text{F}$)
ω	= 350 (rpm)
τ	= 1875.8 (ft-lbf/min)
Q_p	= 20 (ft/hr)
T_{MBH}	= 80 ($^{\circ}\text{F}$)

2.4 Fundamental Hydrate Dissociation Model

2.4.1 Dimensionless Variables

The spatial coordinates are normalized as

$$u = \ln(r/r_w)/\ln(r_e/r_w), \quad r_w < r < r_e \quad (17)$$

and

$$v = z/H, \quad 0 < z < H \quad (18)$$

Two advantages realized from these transformations are:

1. When u is discretized, the closely spaced grid points result near the inner boundary where the solution changes rapidly, and
2. the rectangular domain ($r_w < r < r_e$) and ($0 < z < H$) is mapped to a square in the region ($0 < u < 1$) and ($0 < v < 1$).

Prior to defining a dimensionless time, the thermal diffusivities of each zone are determined.

Hydrate Zone:

$$(\rho C_p)_H = (1-\phi) \rho_R C_p_R + \phi \rho_H C_p_H \quad (19)$$

$$K_H = K_R \left[\frac{\phi^{2/3} (\delta_H - 1) + 1}{(\delta_H - 1)(\phi^{2/3} - \phi) + 1} \right] \quad (20)$$

where

$$\delta_H = K_H/K_R \quad (21)$$

$$D_H = K_H / (\rho Cp)_H$$

Dissociated Zone:

$$(\rho Cp)_D = (1-\phi) \rho_R Cp_R + \phi (\rho_w Cp_w S_w + \rho_g Cp_g S_g) \quad (22)$$

The gas density used here is calculated as

$$\rho_g = 2.7 \frac{\gamma_g P_R(z)}{z_g T_f(z)} \quad (23)$$

where $P_R(z)$ is the hydrostatic pressure at the hydrate depth,

$$P_R(z) = 0.435z + 14.7 \quad (24)$$

and $T_f(z)$ is the hydrate dissociation temperature (methane hydrates),

$$T_f(z) = \frac{15360.8}{37.05 - \ln(P_R(z))} - 459.7 + a_{fx} \quad (25)$$

The gas compressibility factor is calculated using the Standing modification of the Brill and Beggs correlation for curve fitting the Standing-Katz z-factor charts (Standing, 1977).

$$K_D = K_R \left[\frac{s_w \{ \phi^{2/3} (\delta_w - 1) + 1 \}}{\{ (\delta_w - 1) (\phi^{2/3} - \phi) + 1 \}} + \frac{s_g \{ \phi^{2/3} (\delta_g - 1) + 1 \}}{\{ (\delta_g - 1) (\phi^{2/3} - \phi) - 1 \}} \right] \quad (26)$$

Where $\delta_w = K_w/K_R$ and $\delta_g = K_g/K_R$.

$$D_D = K_D / (\rho C_p)_D \quad (27)$$

Dimensionless time (Fourier's number) can now be defined for each region, i.e. dissociated hydrate zone, solid hydrate zone, and the overburden and underburden:

$$\tau_{D_i} = D_i t / r_w^2, \quad i = D, S, O \quad (28)$$

Dimensionless temperatures are defined by

$$\theta_i(u, v, \tau_{D_i}) = \frac{[T(u, v, \tau_{D_i}) - T_f(v)]}{[T_w - T_f(v)]} \quad (29)$$

where, $i = D, S, O$

and $T_f(v)$ is given by Equations (24) and (25).

The following dimensionless terms are also defined:

$$\beta = r_e / r_w \quad (30)$$

$$\lambda = [\ln(r_e/r_w)]^2 \quad (31)$$

$$\mu = (r_w/H)^2 \quad (32)$$

$$\epsilon(v) = \frac{T_f^2(v)}{15360.8 H [T_w - T_f(v)]} \times \left[\frac{0.435}{0.435(z - vh) + 14.7} \right] \quad (33)$$

$$\sigma(v) = \left[\frac{0.435}{0.435(z - vh) + 14.7} \right]^2 \times \left[\frac{T_f^2(v)}{15360.8 H^2 [T_w - T_f(v)]} \right] \times \left[\frac{2T_f(v)}{15360.8} - 1 \right] \quad (34)$$

2.4.2 Dimensionless Differential Equations and Boundary Conditions

The dimensionless differential equation describing unsteady-state heat conduction in an isotropic medium can now be expressed as

$$\frac{\beta}{\lambda} \frac{-2u}{\delta u^2} \frac{\delta^2 \theta_1(u, v, \tau_{D_1})}{\delta u^2} + \mu \frac{\delta^2 \theta_1(u, v, \tau_{D_1})}{\delta v^2} - 2\mu \epsilon(v) \frac{\delta \theta_1(u, v, \tau_{D_1})}{\delta v}$$

$$+ \mu\sigma(v)[1 - \theta_i(u, v, \tau_{D_i})] = \frac{\partial \theta_i(u, v, \tau_{D_i})}{\partial \tau_{D_i}} \quad (35)$$

where, $i = D, S, 0$

Initial Condition

$$\theta_i(u, v, 0) = \frac{[T_{in}(v) - T_f(v)]}{[T_w - T_f(v)]} \quad (36)$$

$0 < u < 1, 0 < v < 1, \tau_{D_i} = 0, i = S, 0$

where,

$$T_{in}(v) = (Z - vH - z_{pfb}) G_{th} + 30.2 \quad (37)$$

and

$$z_{pfb} = (30.2 - T_{ms})/G_{fr} \quad (38)$$

Inner Boundary Condition

$$\theta_i(0, v, \tau_{D_i}) = 1, \quad (39)$$

$$u = 0, 0 < v < 1, \tau_{D_i} > 0, i = D, 0$$

Outer Boundary Condition

$$\theta_i(1, v, \tau_{D_i}) = \frac{[T_{in}(v) - T_f(v)]}{[T_w - T_f(L)]} \quad (40)$$

$$u = 1, 0 < v < 1, \tau_{D_i} > 0, i = S, O$$

Upper and Lower Boundary Conditions

$$\frac{\beta^{-2u}}{\lambda} \frac{\partial^2 \theta_0(u, v, \tau_{D_0})}{\partial u^2} = \frac{\partial \theta_0(u, v, \tau_{D_0})}{\partial \tau_{D_0}} \quad (41)$$

$$0 < u < 1, v = 1, \tau_{D_0} > 0$$

$$\frac{\beta^{-2u}}{\lambda} \frac{\partial^2 \theta_0(u, v, \tau_{D_0})}{\partial u^2} = \frac{\partial \theta_0(u, v, \tau_{D_0})}{\partial \tau_{D_0}} \quad (42)$$

$$0 < u < 1, v = 0, \tau_{D_0} > 0$$

Moving Boundary Conditions

1. From temperature continuity considerations,

$$\theta_D(u_f, v_f, \tau_{D_D}) = \theta_S(u_f, v_f, \tau_{D_S}) = \theta_f \quad (43)$$

Where u_f and v_f are the coordinates of any given point on the moving boundary.

2. From the energy balance considerations at the moving boundary,

the Stefan conditions are:

$$\left[1 + \mu \lambda \beta^2 u \left(\frac{du_f}{dv} \right)^2 \right] \left[\frac{K_S}{K_D} \frac{\beta^{-2} u}{\lambda} \frac{\partial \theta_S(u, v, \tau_{D_S})}{\partial u} - \frac{\beta^{-2} u}{\lambda} \frac{\partial \theta_D(u, v, \tau_{D_D})}{\partial u} \right] = \frac{L_f(v)}{C_p D [T_w - T_f(v)]} \frac{du_f}{d\tau_{D_D}} \quad (44)$$

and

$$\begin{aligned} & \left[1 - \frac{\beta^{-2} u}{\mu \lambda} \left(\frac{dv_f}{du} \right)^2 \right] \left[\frac{K_S}{K_D} \left\{ \frac{\partial \theta_S(u, v, \tau_{D_S})}{\partial v} + \epsilon(v) \right\} - \right. \\ & \left. \left\{ \frac{\partial \theta_D(u, v, \tau_{D_D})}{\partial v} + \epsilon(v) \right\} \right] \\ & = \frac{L_f(v)}{C_p D \mu [T_w - T_f(v)]} \frac{dv_f}{d\tau_{D_D}} \end{aligned} \quad (45)$$

where $L_f(v)$ is the latent heat of fusion of the hydrates and is determined by

$$L_f(v) = \phi S_H [10743.1 - 1.9204 T_f(v)] \quad (46)$$

2.4.3 General Solution Method of the Fundamental Hydrate Dissociation Model

The solution of the above problem involves determination of the temperature distribution in each zone and the position of the

moving boundary at any time τ_{Dn} , $n = 0, 1, 2, \dots, N-1$.

In general, it is necessary to solve four separate problems to obtain the solution at time τ_{Dn+1} for the time interval $\Delta\tau_{Dn}$. The first three problems are boundary value problems, the solutions of which give the temperature distribution in each of the zones. The fourth problem consists of two sets of initial value problems, the solutions of which give two sets of vectors \vec{u}_{fp} , $p = 1, 2, \dots, P$ and \vec{u}_{fq} , $q = 1, 2, \dots, Q$ defining the position of the moving boundary. Here P is the number of grid points that the interface intersects grid lines parallel to the u coordinate and Q those parallel to the v coordinate.

The boundary value problems, given in dimensionless form by equations (35) through (43) and written for each zone, are solved using an iterative, semi-implicit line successive over-relaxation technique (LSOR) (Crichlow, 1977). In applying this technique to a particular grid line in the hydrate zone, the temperature distribution is determined first for the dissociated zone, followed by the solid hydrate zone, and then the temperatures along the whole grid line are relaxed.

The two sets of initial value problems given in dimensionless form by equations (44) and (45) are solved by the trapezoidal method.

To advance the solution from τ_{Dn} to τ_{Dn+1} , the algorithm presented by Sengul (1977) is used with slight modification. The major difficulty in obtaining a solution is the evaluation of the initial value problems because it requires an estimation of the temperature gradients at the moving boundary. To evaluate these

temperature gradients, the temperatures of the grid points on either side of the interface and the temperature of the moving boundary are fitted to a polynomial using a least squares method (Gerald and Wheatly, 1984). The degree of polynomial fit to the temperature profiles is allowed to vary from degree 1 to degree 9. The optimum degree of the polynomial is selected by increasing the degree of the polynomial, beginning with degree one, so long as there is a significant decrease in the variance (Gerald and Wheatly, 1984).

Once these polynomials have been determined for the temperature profiles in each of the dissociated and solid hydrate zones in the u direction and in the v direction, Richardson Extrapolation (Cheney and Kincaid, 1985) is used to determine the first derivative of the polynomials, i.e. the temperature gradients at the moving boundary. The details of the solution method are discussed elsewhere (Roadifer, 1987).

2.4.4 Gas Influx Calculations

Once the above problem has been solved for some time period, Δt , a simple material balance is used to calculate the gas influx into the wellbore.

The volume of hydrate dissociated is given by

$$V_H = \pi \phi H_H \{ [r_f(t + \Delta t)]^2 - [r_f(t)]^2 \} \quad (47)$$

The moles of methane gas originally contained in this volume is

$$n_{gH} = \frac{181.3}{379.5} V_H \quad (48)$$

The moles of methane gas the dissociation volume would contain at wellbore conditions is

$$n_{gwB} = \frac{P_F V_H S_g}{z_g R T_m} \quad (49)$$

2.5 Summary and Conclusions

A comprehensive wellbore hydraulics and heat transfer model and a fundamental hydrate dissociation model has been developed. The model development allows the detailed examination of the effects of a wide range of drilling parameters on the wellbore pressure, wellbore temperature and, consequently, hydrate dissociation rate for arctic terrestrial, arctic subsea and subtropic subsea locations.

2.6 NOMENCLATURE

- a_{fx} = freezing point depression of hydrates due to dissolved solids
- C_p = specific heat ($\text{Btu/lb}^{\circ}\text{F}$)
- D = diameter (inches) or thermal diffusivity (ft^2/hr)
- E_{fr} = frictional energy losses (Btu/ft hr)
- E_{rot} = rotational energy (Btu/ft hr)
- f = positin of the interface
- g_G = geothermal gradient ($^{\circ}\text{F}/\text{ft}$)
- G_{fr} = geothermal gradient within permafrost ($^{\circ}\text{F}/100 \text{ ft}$)
- G_{th} = geothermal gradient below permafrost ($^{\circ}\text{F}/100 \text{ ft}$)
- h = convective heat transfer coefficient ($\text{Btu/hr}^{\circ}\text{F ft}^2$)
- H = zone thickness (feet)
- k = thermal conductivity ($\text{Btu/ft hr}^{\circ}\text{F}$)
- L_f = latent heat (Btu/lb)
- M = number of space intervals in both the u and v directions
- MU = number of grids in the underburden in the v direction
- N = total number of time steps
- N_{Re} = Reynold's number
- N_{Nu} = Nusselt number
- p = number of intersections of the moving boundary with grid lines parallel to the u coordinate
- P = pressure (psia)
- Pr = Prandtl number
- ppr = natural log of pressure
- q = flow rate (gal/min)
- Q = heat energy source term (Btu/ft hr)
- Q = gas influx rate (scf/min)

Q = number of intersections of the moving boundary with grid lines parallel to the v coordinate
 QP = formation penetration rate (ft/hr)
 r = radius (feet)
 r_e = radius to the outer boundary
 r_f = radius to the moving boundary (front)
 r_n = dimensionless variable defined as $\Delta\tau_D/(\Delta u)^2 = \Delta\tau_D/(\Delta u)^2$
 s = wellbore radius
 S = Surface
 St = Stanton number
 t = time (hours)
 T = temperature ($^{\circ}$ F)
 T_{bpf} = temperature at the base of the permafrost
 T_{in} = initial temperature distribution
 u = normalized radial direction
 u_f = dimensionless radial position of the moving boundary
 v = normalized vertical direction
 V = Volume
 V = velocity (ft/s)
 v_f = dimensionless vertical position of the moving boundary
(below inflection point)
 z = depth (ft.)

Greek Symbols

α = thermal diffusivity (ft 2 /hr)
 α = curvilinear coordinate transformation variable
 β = hydrate gas content (SCF/ft 3 hydrate)

β = dimensionless variable defined in Equation 30
 γ = curvilinear coordinate transformation variable
 ϵ = dimensionless variable defined by Equation 33
 θ = 1. angle
= 2. dimensionless temperature
 λ = dimensionless variable defined by Equation 39
 σ = dimensionless variable defined by Equation 41
 ρ = density (lb/ft^3)
 μ = viscosity (cp)
 ϕ = porosity
 τ = dimensionless time (Fourier's Number)
 τ = torque ($\text{ft lb}_f/\text{min.}$)
 ψ = domain
 ω = angular velocity (rpm)
 ω = relaxation parameter

Superscripts

n = time level

Subscripts

a = annulus

BH = bottom hole

c = casing

ce = cement

D = dissociated (thawed) zone

DH = dissociated hydrate zone

D_p = thawed permafrost zone

e = extent of reservoir (formation)

for = formation

f_H = hydrate dissociation front
 f_p = permafrost thaw front
 H = hydrate
 i = radial grid index
 in = initial
 j = vertical grid index
 j_{max} = bottom-most grid
 k = index of iteration
 k = region indication (i.e. casing, cement, thawed permafrost, unthawed permafrost, formation, dissociated hydrate, undissociated hydrate)
 l = discrete index of v direction
 m = discrete index of v direction
 m_{eq} = equivalent annulus mud
 m_i = mud in
 m_s = mean annual surface
 o/u = overburden or underburden zone
 p = number of points where the moving boundary intersects the grid lines in the radial direction
 p = permafrost
 p_i = inside drill pipe
 p_{fb} = permafrost base
 p_o = outside drill pipe
 q = number of points where the moving boundary intersects the grid lines in the vertical direction
 S = solid region
 SH = solid hydrate
 Sp = unthawed permafrost
 w = drill pipe (collar) wall

wat = water

wb = wellbore

2.7 REFERENCES

- Bourgoyne, A.T. Jr., Chenevent, M.E., Millheim, K.K., and Young, F.S. Jr.: Applied Drilling Engineers, SPE Textbook Series, Vol. 2, (1986).
- Cheney, W. and Kincaid, D.: Numerical Mathematics and Computing, Brooks/Cole Publishing Company, Monterey, California, 2nd Edition (1985).
- Crichlow, H.B.: Modern Reservoir Engineering - A Simulation Approach, Prentice-Hall, Inc., Englewood Cliffs, NJ (1977).
- Gerald, C.F. and Wheatley, P.O.: Applied Numerical Analysis, Addison-Wesley Publishing Company, Reading, Massachusetts, 3rd Edition (1984).
- Incropera, F.P. and Dewitt, D.P.: Fundamentals of Heat Transfer, John Wiley and Sons, New York (1981).
- Keller, H.H., Couch, E.J., and Berry, P.M.: "Temperature Distribution in Circulating Mud Columns", Society of Petroleum Engineers Journal, pp 23-30, (Feb. 1973).
- Lakshminarayanan, M.S., Lalchandari, R., and Raja Rao, M.: "Turbulent Flow Heat Transfer in Circular Tubes", Indian Journal Tech., Vol. 14, pp 521-525, (1976).
- Marshall, D.W. and Bentsen, R.G.: "A Computer Model to Determine the Temperature Distributions in a Wellbore", Journal of Canadian Petroleum Technology, pp 63-75, (Jan. - Feb., 1982).
- Roadifer, R.D., "A r-z Unsteady State Simulator for a Stefan Problem with Variable Thermal Conductivity", M.S Thesis, University of Alaska, Fairbanks, Alaska 99709 (1987).
- Sengul, M.: Numerical Solution of Heat Conduction with Phase Change in Cylindrical Systems, Ph.D. Dissertation, Dept. of Petroleum Engineering, Stanford University, California (1977).
- Standing, M.B.: Volumetric and Phase Behavior of Oil Field Hydrocarbon Systems, Society of Petroleum Engineers of AIME, Dallas, Texas pp. 121-122 (1977).

2.8 APPENDIX A

A. Determination of Convective Heat Transfer Coefficient

For laminar flow of any type of fluid, i.e. Newtonian, Bingham Plastic, or Power Law, the Newtonian value of 4.12 for the Nusselt is number used:

$$\text{Laminar: } N_{Nu} = 4.12 \quad (1A)$$

For turbulent flow of Newtonian fluids or Bingham Plastics, the Seider-Tate equation is used with the following term $(\mu/\mu_w)^{0.14}$ set equal to 1 (Incropera and Dewitt, 1981). For Bingham Plastics, the plastic viscosity is used to calculate the Reynold's and Prandtl numbers.

$$\text{Turbulent: } N_{Nu} = 0.027 N_{Re}^{0.8} \Pr^{0.333} \quad (2A)$$

Marshall and Bentsen (1982) recommend the use of a correlation developed by Lakshminarayanan et al (1976) for power-law fluids in turbulent flow:

$$St = 0.0107 N_{Re}^{-0.33} \Pr^{-0.67} \quad (3A)$$

In annular flow, the hydraulic diameter of the annulus should be used in these correlations, and the equivalent fluid properties accounting for the drill cuttings and fluid influx into the wellbore should also be used.

B. Determination of Energy Source Terms

The source of heat generation within the wellbore system is a result of the rotational energy due to the work required to rotate the drill string, viscous energy due to frictional losses within the drill pipe, drill bit and annulus, and the work done by the bit.

The thermal energy generated due to rotation and work by the drill bit is calculated by assuming that all of the mechanical energy input by the rotating drive is converted to thermal energy. This energy is then divided 60% to the drill pipe and 40% to the drill bit. The rotational energy input may be calculated by Equation (4A):

$$E_{\text{rot}} = 0.4844 \text{ wt} \quad (4A)$$

The total thermal energy generated due to frictional pressure losses in the system may be calculated as

$$E_{\text{fr}} = 1.4843 \Delta P_{\text{fr}} q_m \quad (5A)$$

This energy is then divided among the drill string, drill bit and annulus by the ratios of their respective frictional pressure losses.

3.0 DEVELOPMENT OF GUIDELINES FOR DRILLING IN THE PRESENCE OF HYDRATES

Prior to establishing guidelines for drilling through hydrate containing formations, a parametric study of the reservoir property and drilling parameter effects on hydrate dissociation is required. In addition, potential hydrate precautions can be taken to avoid the problems associated with drilling through those zones.

3.1 Hydrate Stability Zones

With the knowledge of geothermal gradients, pressure - depth - temperature diagrams can be constructed to identify the depths at which gas hydrates may be present. Several thermodynamic studies on the measurement of pressure-temperature relationships for different gas hydrates have been reported in the literature (Deaton and Frost, 1946; Kobayashi and Katz, 1955; Holder, 1976; Wu et al, 1976; Kamath, 1982; Holder and Hand, 1983) and serve as the basis for determination of hydrate stability. Kamath et al (1987) have studied the effects of various parameters on hydrate stability in regions of permafrost. The knowledge of mean annual ground temperature, geothermal gradient, pressure gradient and gas composition is required to fully evaluate potential zones of hydrate occurrence. Other factors influencing hydrate stability include salinity of pore fluids, pore pressure conditions and soil particle effects. Godbole et al (1987) extended the work of Kamath et al (1987) to develop a nomogram (Figure 1) to determine the depths of potential hydrate zones for the wide range of conditions that exist on the North Slope of Alaska and can

be expected to occur in other arctic regions.

Using data from McCleod and Campbell (1961) for sea temperatures, Roadifer et al (1987) extended the work of Godbole et al (1987) and Kamath et al (1987) to develop two additional diagrams (Figure 2 & 3) for determining depths of potential hydrate stability zones in both arctic subsea and subtropic subsea locations. The only requirements for using these diagrams are the sea depth and an estimation of the geothermal gradient below the sea floor. The two main assumptions made in developing diagrams are: the pressure gradient is hydrostatic; and, the hydrates are composed of water and methane only.

3.2. Reservoir Parametric Study

Using a two-dimensional ($r-z$) cylindrical coordinate thermal hydrate dissociation simulator, Roadifer et al (1987) performed a parametric study of the effects of various reservoir and wellbore parameters on hydrate dissociation rates in arctic regions underlain by permafrost. Parameters studied included: mean annual surface temperature; depth to permafrost base; geothermal gradient within permafrost; geothermal gradient below permafrost; hydrate zone depth; hydrate zone thickness; reservoir porosity; wellbore radius; bottomhole temperature; and equivalent circulating mud density effects on gas influx.

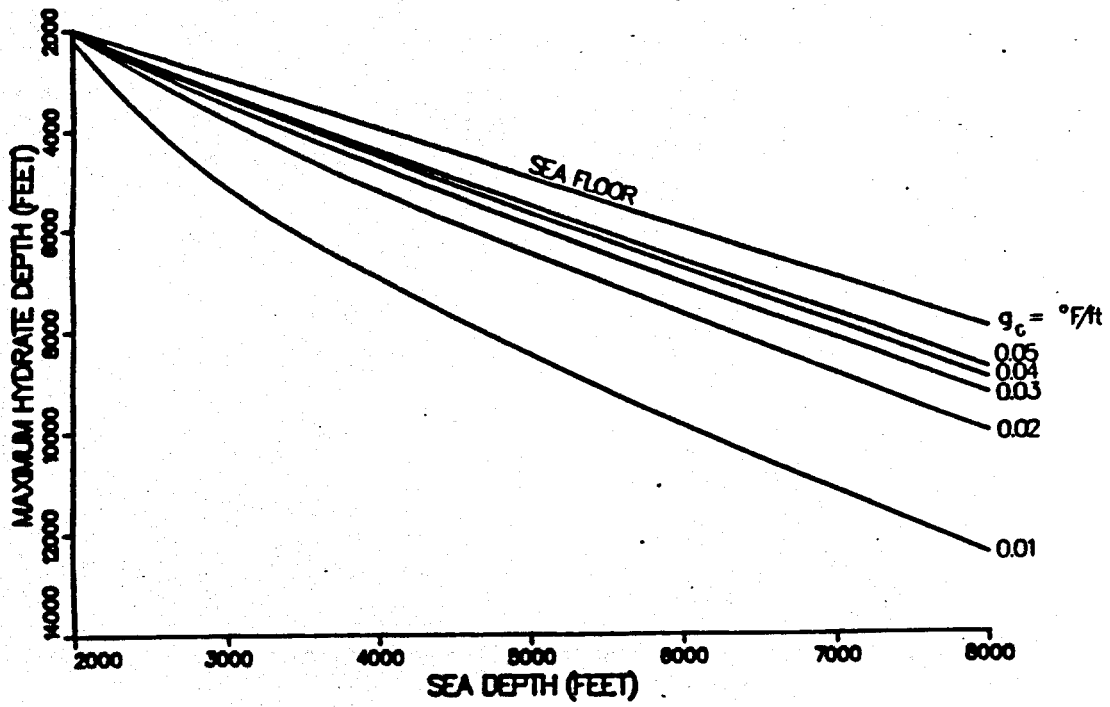


Figure 2: Zone of Hydrate Stability in
the Arctic Subsea Region

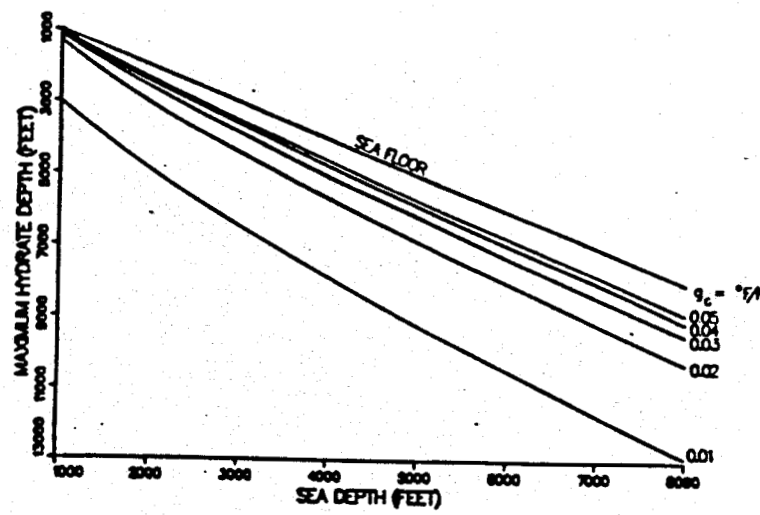


Figure 3: Zone of Hydrate Stability in the Subtropic Subsea Region

3.2.1 Geothermal Conditions

While important for establishing potential hydrate stability zones, the geothermal parameters, i.e., mean annual surface temperature, depth to permafrost base, and geothermal gradients within and below the permafrost, were found to have negligible effects on the hydrate dissociation rate. This was seen to indicate that heat transfer occurs predominately in the dissociated hydrate zone with the sensible heat required to raise the solid hydrates to dissociation temperature being negligible.

3.2.2 Hydrate Zone Depth

The effect of the hydrate zone depth on the rate of hydrate dissociation is illustrated in Figure 4. The non-linearity of the relationship is explained by the non-linear effect of pressure on the hydrate dissociation temperature, i.e., a hydrostatic pressure gradient was assumed and the hydrate dissociation temperature varies inversely to a logarithmic function of pressure. Because the hydrate dissociation temperature increases with an increase in pressure (depth), the rate of heat transfer, and therefore, hydrate dissociation rate decreases for a fixed wellbore temperature.

3.2.3 Hydrate Zone Thickness

Hydrate zone thickness shows negligible effect on the rate of hydrate dissociation probably due to negligible heat transfer from the overburden and underburden for the thickness range considered. The total hydrates dissociated, however, and

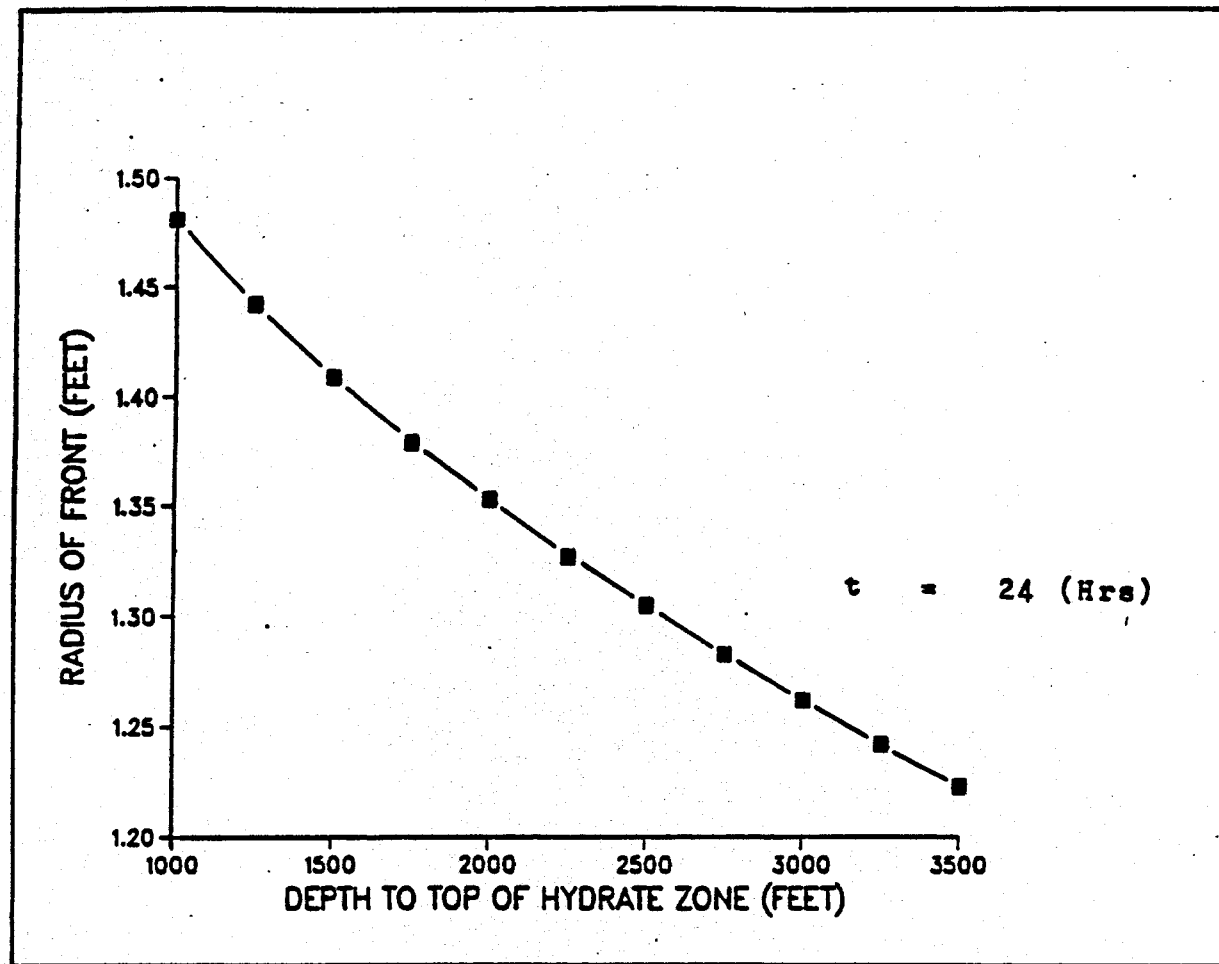


Figure 4 : Effect of Depth of Hydrate on Dissociation Rate

therefore, the surface gas realized are affected directly by the hydrate zone thickness as indicated in Figure 5.

3.2.4 Porosity

The relationship between porosity and hydrate dissociation rate as indicated by the surface gas rate is shown in Figure 6. While significant, this relationship is slightly exaggerated due to the expanded y-axis scale. The maximum difference in hydrate dissociation rates is about 22 percent between the lowest rate at 45 percent porosity and the high at 20 percent porosity.

The increase in the hydrate dissociation rate with a decrease in porosity (down to approximately 20 percent) is due to an increase in the thermal conductivity of the dissociated zone which, because of the fixed wellbore temperature, results in an increase in the heat transfer rate from the wellbore into the dissociated zone.

At the same time, however, the sensible heat required to heat the reservoir rock also increases, but at a different rate. The maximum dissociation rate occurs when for a given reduction in porosity the increase in the heat transfer rate just equals the additional sensible heat required to heat the reservoir rock. For porosities lower than this maximum the additional heat required to heat the reservoir rock is greater than the additional heat supplied to the system.

3.2.5 Drilling Parameter Analysis

The rate of hydrate dissociation depends strongly on the

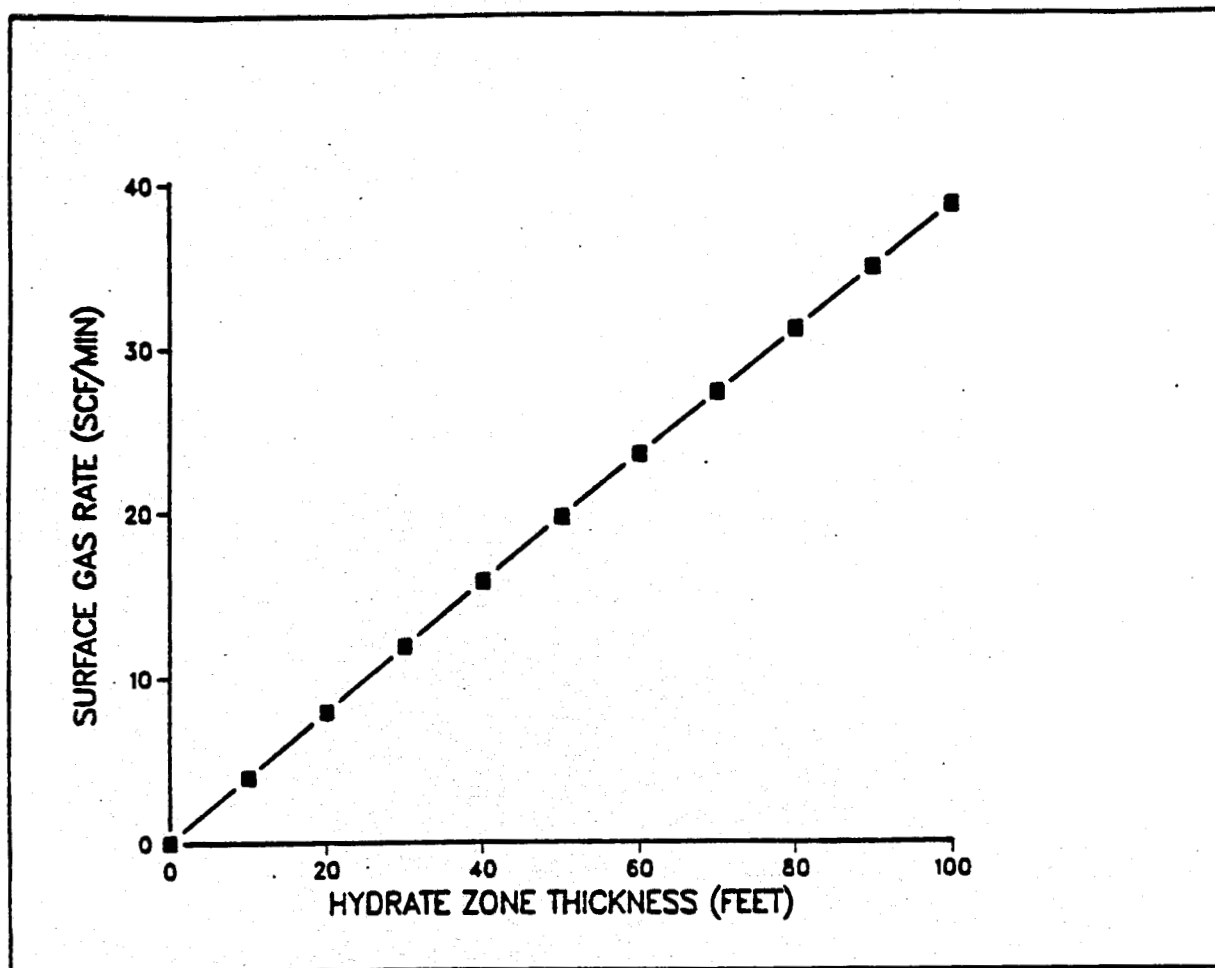


Figure 5: Effect of Hydrate Zone Thickness on Gas Influx Rate

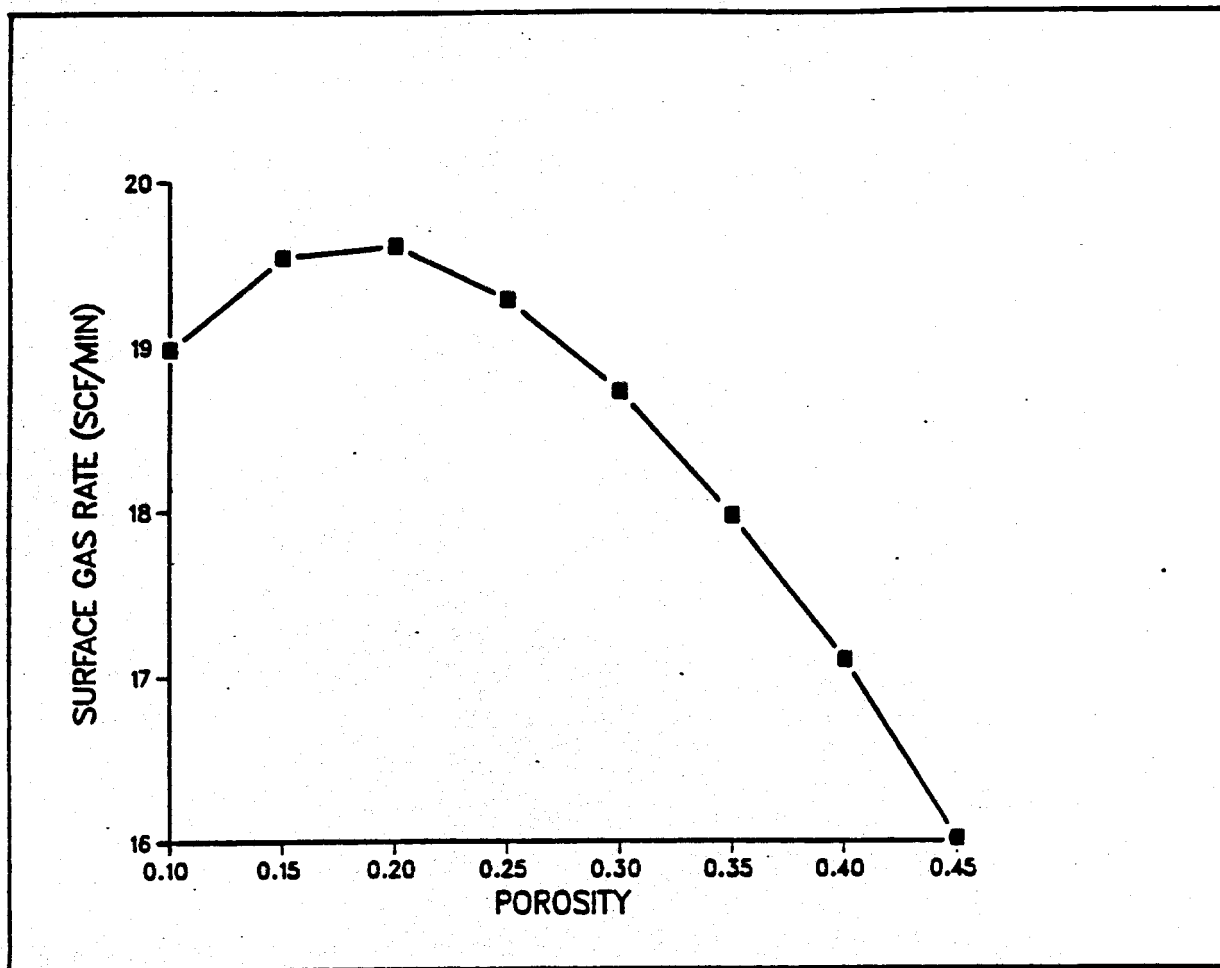


Figure 6: Relationship Between Porosity and Dissociation Rate

wellbore temperature and the pressure exerted at the hydrate -- dissociated zone interface (both the dissociation temperature and latent heat of dissociation are functions of pressure). The relationship between these two variables and the hydrate dissociation rate (as shown by the surface gas rate) is shown in Figure 7. It should be noted that in addition to affecting the hydrate dissociation rate, the wellbore pressure also affects the gas influx rate from the formation into the wellbore. The pressure effects noted in Figure 7 include both the dissociation rate effect and the gas influx effect.

The effect of pressure on the gas influx rate can be implied from Figure 8 which includes only this effect for various mud densities. This figure indicates that the pressure effect on the gas influx rate is minimal, causing only a minor reduction in the gas influx rate with increased mud density and, therefore, pressure.

3.2.6 Wellbore Radius

In addition to the wellbore temperature and pressure, the wellbore radius also affects the hydrate dissociation rate as indicated by Figure 9. The effect of the wellbore radius on the hydrate dissociation rate is due to an increase in the heat transfer rate with an increase in the wellbore radius. While variations in this parameter are usually not at the discretion of the drilling engineer, the wellbore radius does have a significant effect on the hydrate dissociation rate.

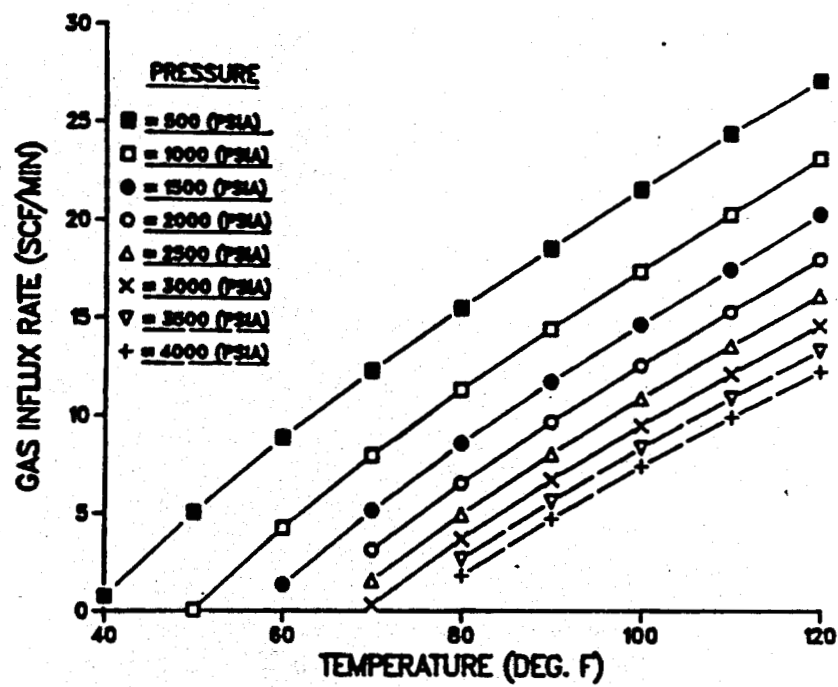


Figure 7: Effect of Temperature and Pressure on the Hydrate Dissociate Rate

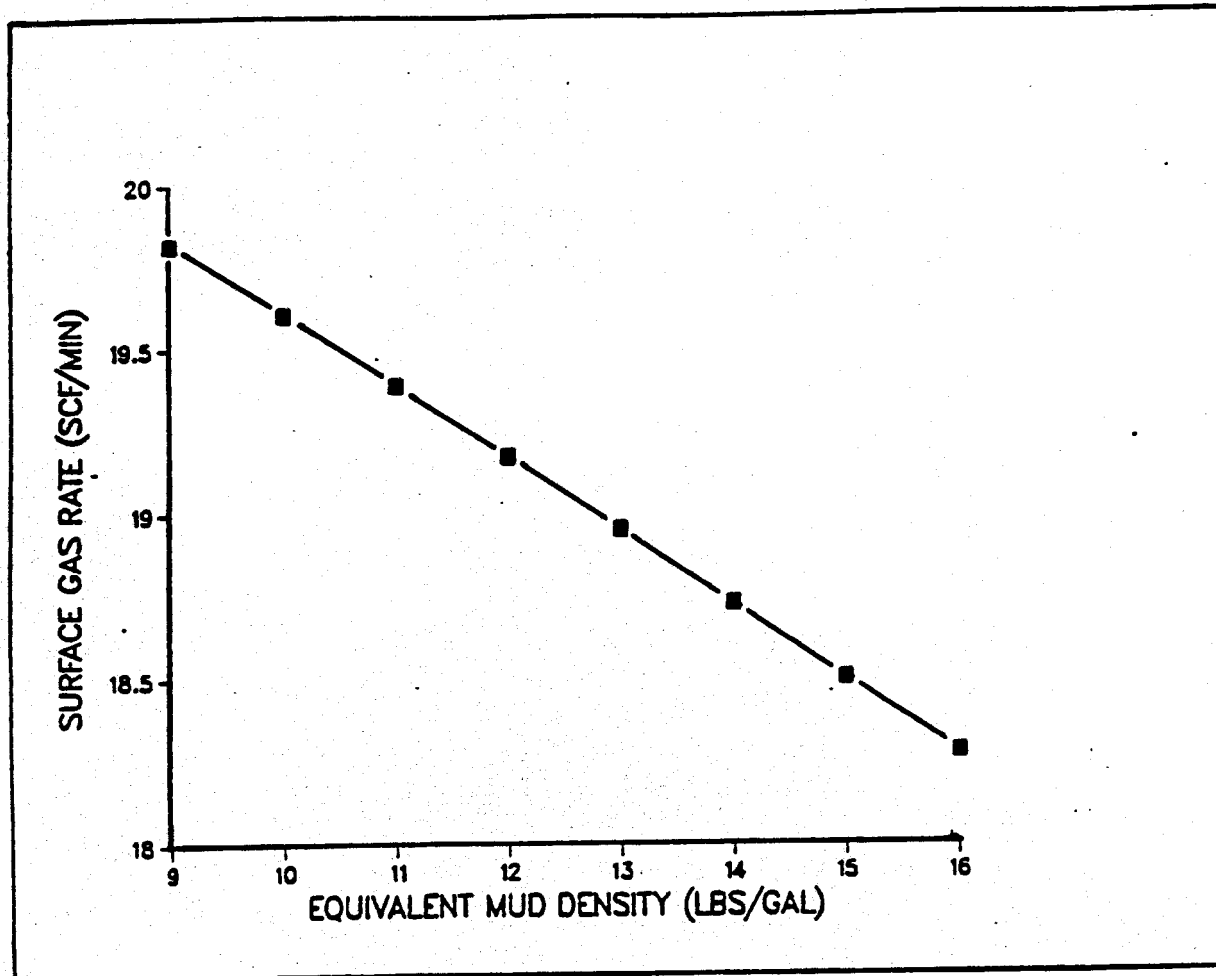


Figure 8: Effect of Mud Density on Gas Influx Rate

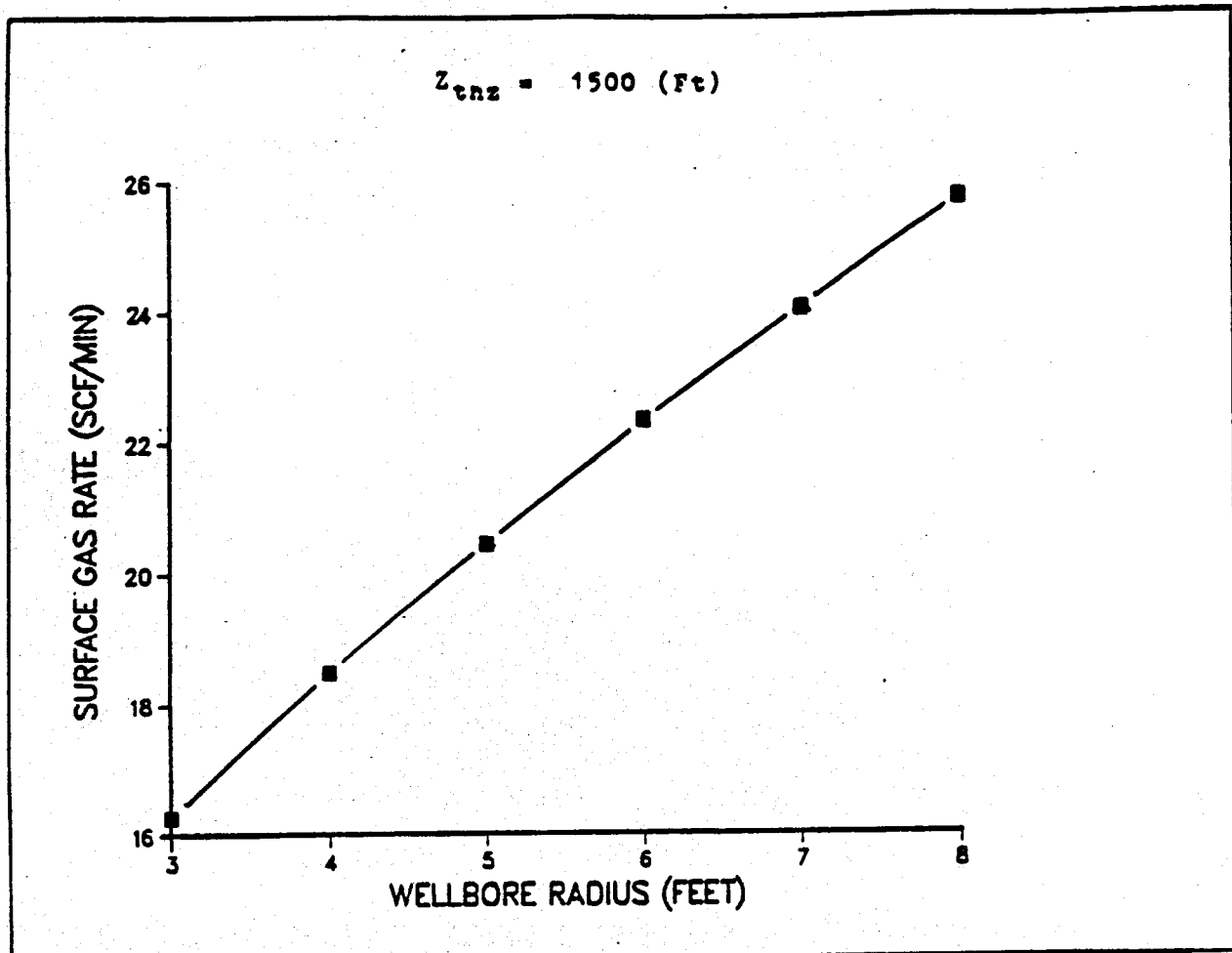


Figure 9: Effect of Wellbore Radius on Dissociate Rate

3.2.7 Pressure

The drilling and mud engineers have control over three variables which affect the pressure exerted against the formation in the wellbore. These variables are the mud density, viscosity, and circulation rate. The absolute benefits and disadvantages (eg., economics, cutting, removal, etc.) of varying each of these parameters are beyond the scope of this study, but they are covered adequately in most any drilling or mud engineering text. We only concern ourselves here with the relative effects each of these parameters has on the wellbore pressure.

Increase in any one of these parameters will increase the wellbore pressure. Increasing mud weight has the direct effect of increasing the hydrostatic pressure and though less obvious, the frictional pressure drop. The circulation rate and mud viscosity only affect the frictional pressure drop.

Figure 10 shows the relative effects of mud density and circulation rate on the bottomhole pressure. The figure indicates that a drastic increase in the circulation rate is required to achieve the same pressure as the one attained by small increases in mud weight.

There is an additional advantage, however, to increasing the circulation rate. When the hydrates dissociate into gas and water, some of the gas will enter the wellbore, thus reducing the hydrostatic pressure of the mud column. The amount of gas existing in the mud column will be reduced and, therefore, the hydrostatic pressure maximized if the gas entering the wellbore is circulated out as fast as possible. A quantitative analysis

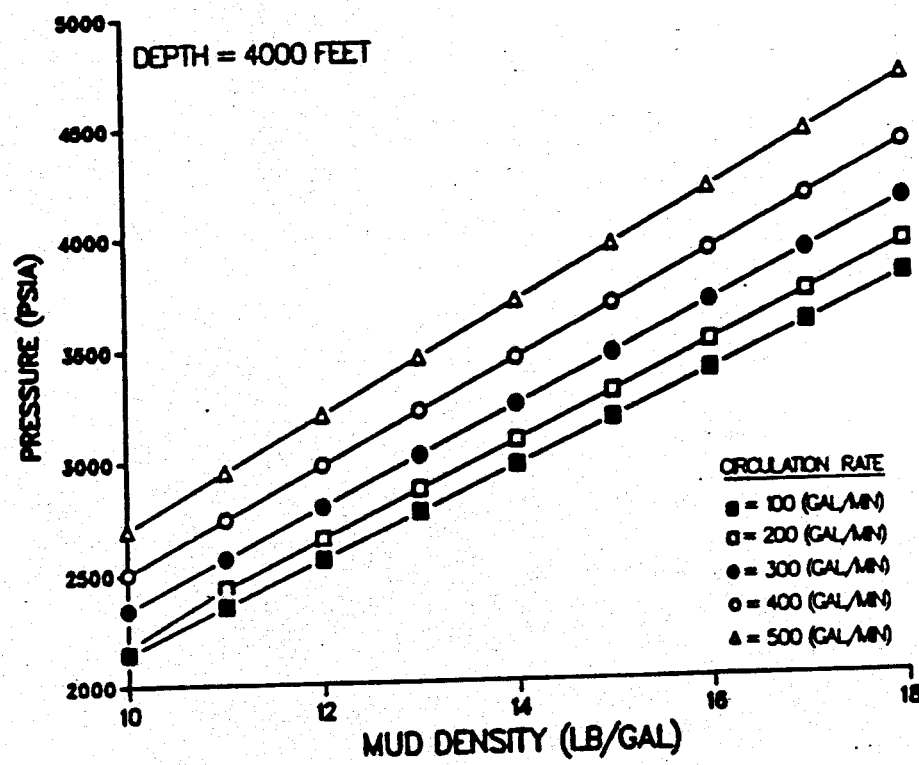


Figure 10: Effect of Mud Density and Circulation Rate on the Bottomhole

of this phenomenon has not been performed at this time.

Figure 11 compares the effects of increasing the mud viscosity and the mud density. Noted here is that large variations in viscosity are required to achieve the same wellbore pressure as moderate increases in the mud weight.

3.2.8 Temperature

The wellbore annulus temperature profile is a function of many variables. As with the wellbore pressure, we concern ourselves here only with those parameters that may be controlled directly by the drilling or mud engineers. A discussion of other variables is available in the literature (Edwardson et al, 1962; Tragesser et al, 1967; Holmes and Swift, 1970; Keller et al, 1973; Marshall and Bentsen, 1982; Corre et al, 1984; and Thompson, 1985).

The primary parameters of concern are the mud inlet temperature, density, circulation rate, and whether or not the hole has been cased. Figure 12 shows a comparison of the bottomhole temperatures generated due to inlet mud temperature for an uncased well and a well cased to the permafrost base. Two noteworthy effects are seen in this plot. First, the change in the bottomhole temperature is much less than the change in the mud inlet temperature. Second, casing the permafrost zone results in significantly higher bottomhole temperatures.

The ramifications of these results depend on the particular method of hydrate control being used, i.e., limiting or promoting

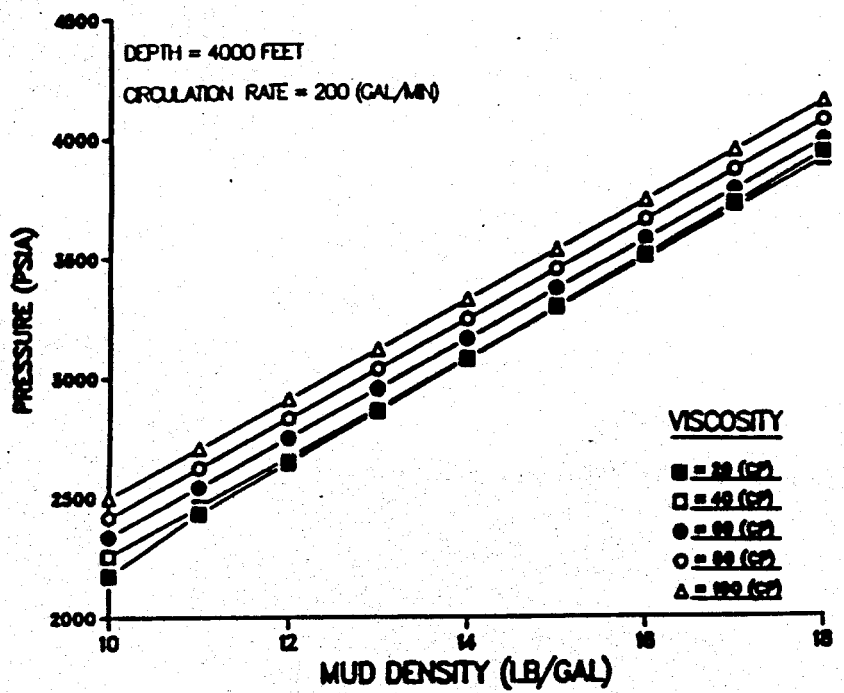


Figure 11: Effect of Mud Density and Viscosity on the Bottomhole Pressure

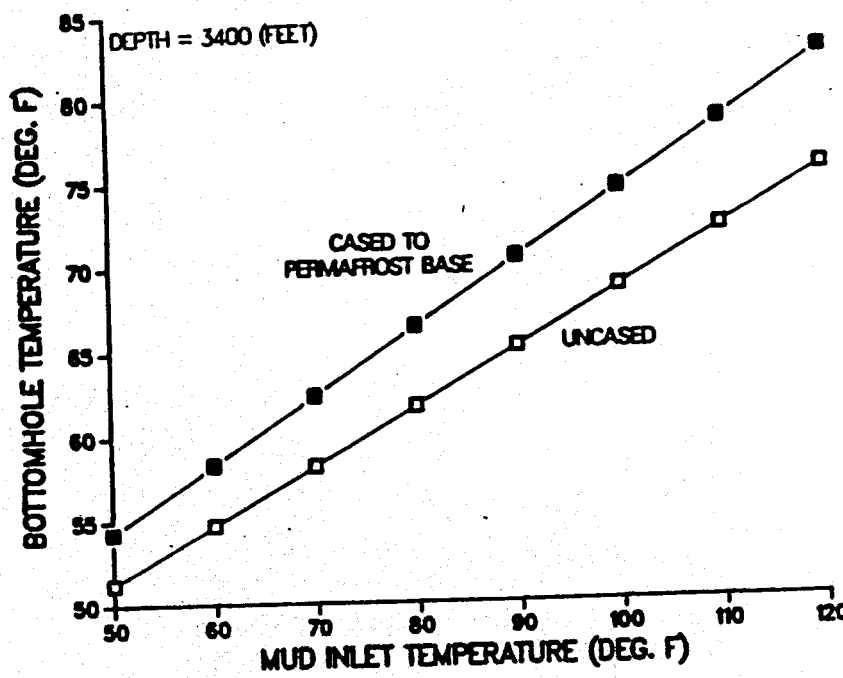


Figure 12: Effect of Casing and Mud Inlet Temperature on the Bottomhole Temperature

hydrate dissociation. If the goal is to limit hydrate dissociation, casing should not be run until the potential hydrate bearing depths have been drilled, assuming this will not cause significant new problems in the permafrost region. In subsea locations, the corollary to this is not to use a riser casing so the cooling effect of the sea can be taken advantage of. If the goal is to promote hydrate dissociation while drilling, the current practice of casing off the permafrost zone as soon as it has been penetrated should be followed.

The effect of mud density and circulation rate on bottomhole temperature is a much more complex problem as indicated by Figure 13. To understand the implications of this figure, a discussion of the heat transfer mechanisms present in the wellbore is required.

Within the wellbore, heat transfer occurs due to vertical convection down the drill string and up the annulus, radial convection between fluid, pipe wall and formation, and lastly due to heat generation. When the mud circulation is increased, vertical convection increases, tending to increase the bottomhole temperature; because the boundary layer convection coefficient increases, radial heat convection increases, tending to decrease the bottomhole temperature; lastly, the frictional pressure drop increases, resulting in higher heat generation and an increase in temperature.

An example will help to clarify these mechanisms. Consider the case of the 14 lb/gal mud in Figure 13. At a circulation rate of 100 gal/min, the flow regime is laminar in both the drill

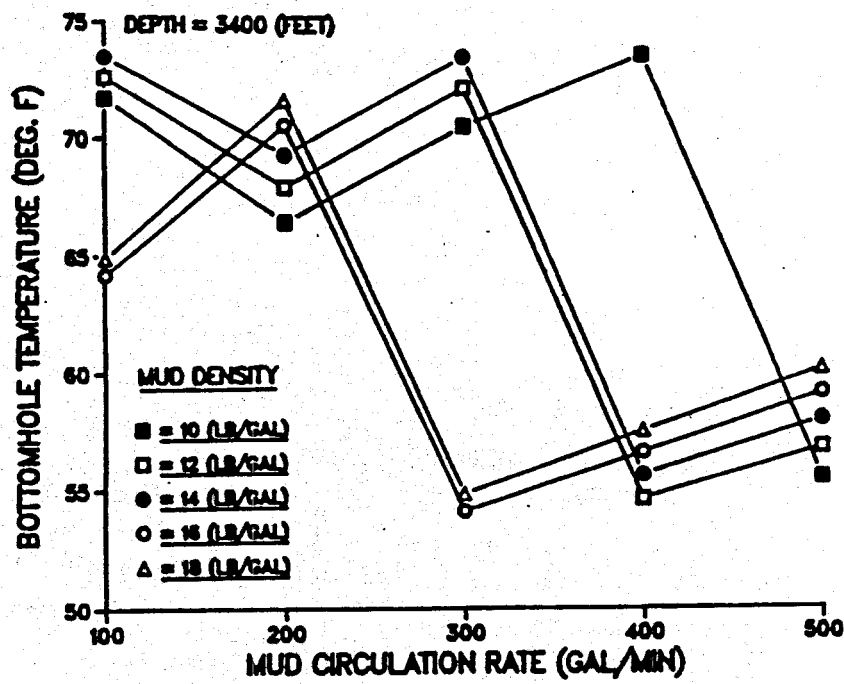


Figure 13: Effect of Mud Density and Circulation Rate on the Bottomhole Temperature

string and the annulus. When the flow rate is increased to 200 gal/min, the flow inside the drill string becomes turbulent, and the convective heat transfer coefficient increases from 8.4 to 146 (Btu/ft²-hr-F). The flow in the annulus, however, has remained laminar with no change in the convective heat transfer coefficient. The heat transfer, therefore, has remained constant between the formation and the annular fluid, whereas heat transfer has increased markedly between the cooler annular fluid and warmer drill string fluid, resulting in the observed temperature drop.

Increasing the flow rate to 300 gal/min results in an additional increase in the drill string convection coefficient (to 200 Btu/ft²-hr-F, a 38% increase), but is counteracted by a 38 percent increase in the heat generation or source term (from 40.3 to 55.6 Btu/ft-hr) and an increase in the vertical convection. This results in a slight increase in the bottomhole temperature. As the flow rate is increased to 400 gal/min, the bottomhole temperature is dramatically reduced. The reason for this sharp drop is quite simple; the flow regime in the annulus has become turbulent, resulting in an increase in the wellbore convective heat transfer coefficient from 28 to 348 (Btu/ft²-hr-F) and a corresponding increase in the heat losses to the formation. As the flow rate is again increased, the effects of vertical convection and heat generation once again become significant.

The above discussion provides guidelines for selection of a flow regime for the drilling fluid. If the goal is to prevent hydrate dissociation, the drilling fluid should be in the

turbulent flow regime in the annulus. If the goal is to promote hydrate dissociation, a laminar flow regime is desired in the annulus.

3.3. Selection of Parameters

The relative effects of many drilling and mud parameters on the wellbore pressures and temperatures (and therefore hydrate dissociation rate and gas influx rate) have been shown and discussed. The precise combination of these parameters to be used to achieve the desired results cannot be stated as each new well is unique and controlled by many factors, e.g., economics, legal restrictions, equipment availability, etc. What can be stated, however, is the temperature and pressure necessary to keep hydrate dissociation within the limits of the drilling equipment, or vice versa, design criteria for the surface degassing equipment can be established for the maximum temperatures and minimum pressures expected to occur over the hydrate zone. These results are presented in nomogram form in Figure 14-16, which represent three different uses of the nomogram. Example uses of the nomogram are presented in the appendix.

Figure 14: Nomogram for Estimation of Parameters For Drilling Through Hydrates

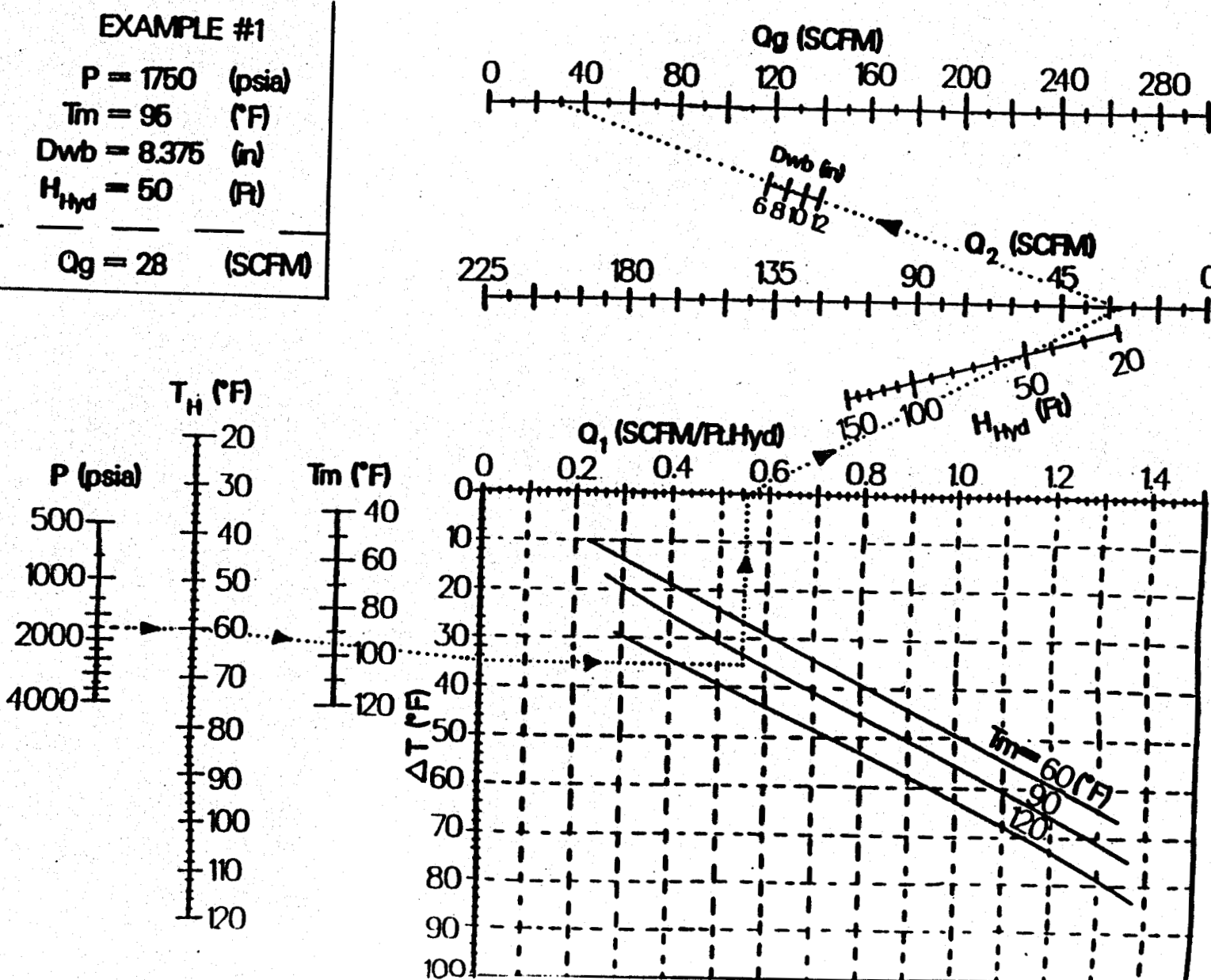
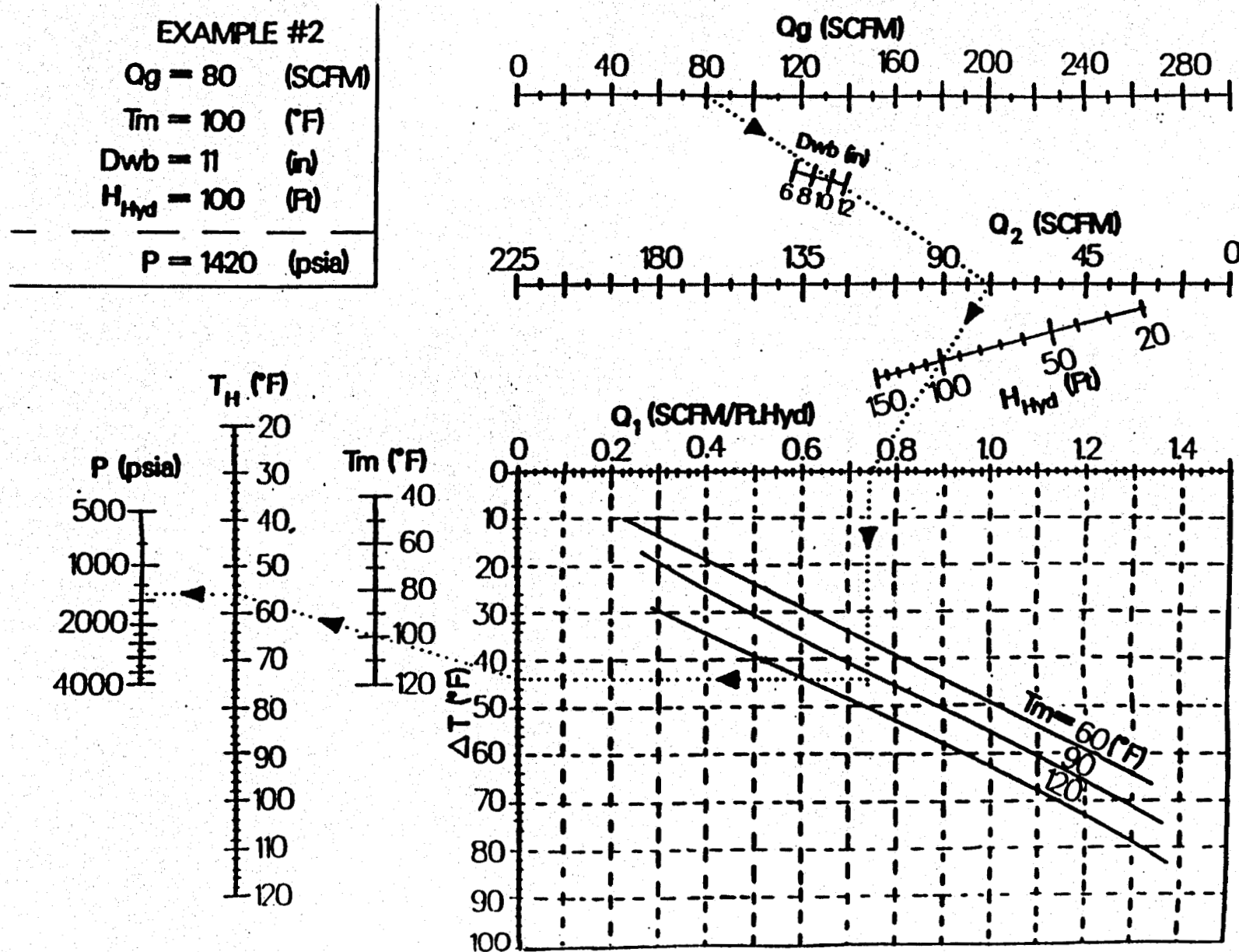


Figure 15: Nonogram for Estimation of Parameters for Drilling Through Hydrates



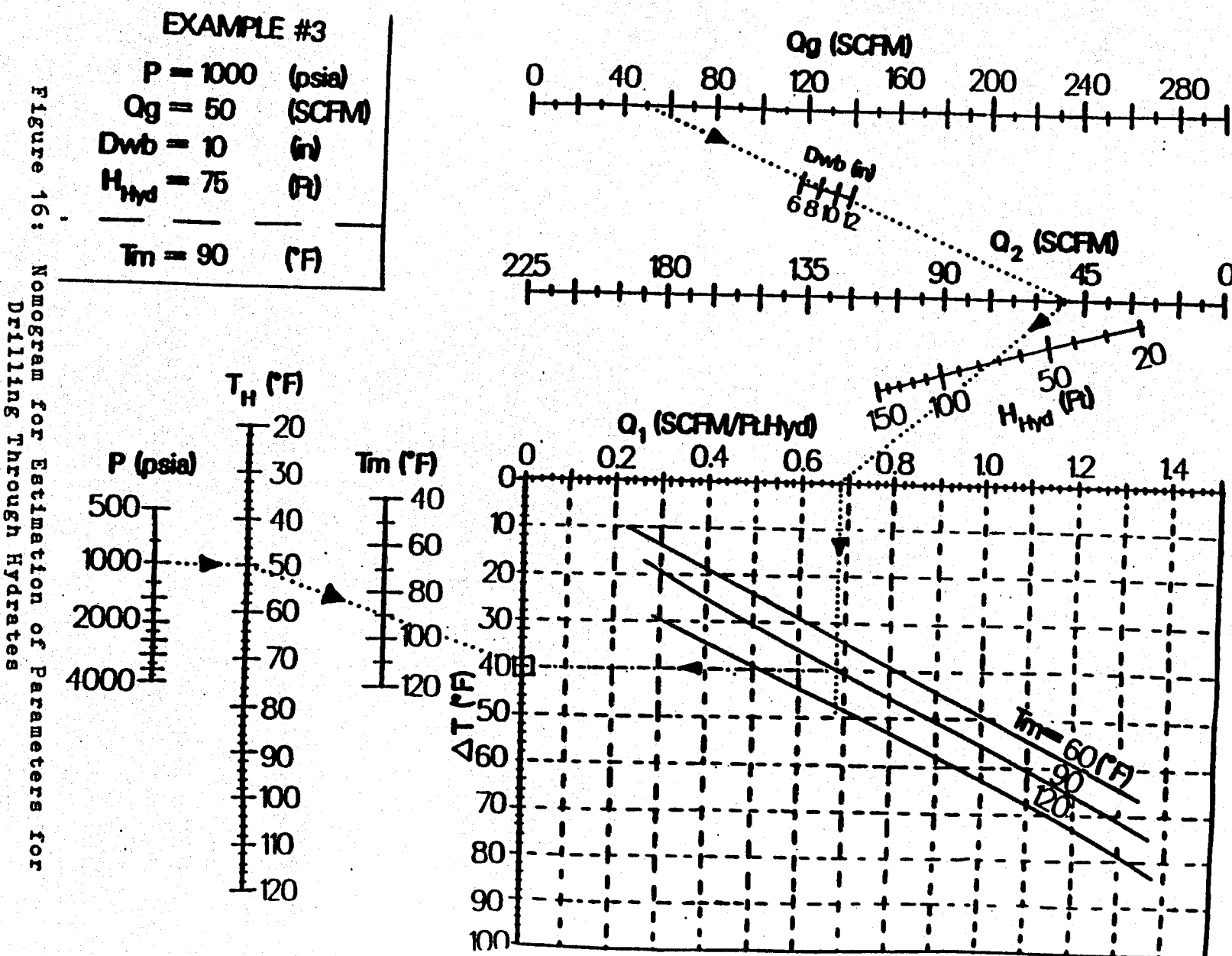


Figure 16: Nonogram for Estimation of Parameters for Drilling Through Hydrates

3.4 References

- Corre, B., Eymard, R., and Guenot, A.: "Numerical Computation of Temperature Distribution in a Wellbore While Drilling", SPE Paper 13208, presented at the 59th Annual Technical Conference and Exhibition, Houston, TX, Sept. 16-19, 1984.
- Deaton, W.M. and Frost, E.M.: "Gas Hydrates and Their Relations to the Operation of Natural Gas Pipelines", U.S. Bureau of Mines, Mongraph-8:108 (1946).
- Edwardson, M.J., Girnen, H.M., Parkison, H.R., Williamson, C.D., and Mathews, C.S.: "Calculation of Formation Temperature Disturbances Caused by Mud Circulation", Jour. Pet. Tech., pp. 416-426 (April 1962).
- Godbole, S.P., Kamath, V.A. and Ehlig-Economides, C.E.: "Natural Gas Hydrates in the Alaskan Arctic", to be published SPE Reservoir Engineering (1987).
- Holder, G.D. and Hand, J.H.: "Mutliphasic Equilibria in Hydrates from Methane, Ethane, Propane and Water Mixtures", AICHE Journal, 28 (3):44, (1983).
- Holder, G.D.: Multiphasic Equilibria in Methane-Ethane-Propane-Water Hydrate Forming Systems, Ph.D. Dissertation, School of Chemical Engineering, University of Michigan, Ann Arbor, Michigan (1976).
- Holmes, C.S. and Swift, S.C.: "Calculation of Circulating Mud Temperatures", Jour. Pet. Tech., pp. 670-674 (June 1970).
- Kamath, V.A.: Dissociation Pressure of Hydrates of Propane, Cis 2-Butane, Trans 2-Butene, Propane/n-Butene and Propane/Trans 2-Butene Mixtures Below the Ice Point, M.S. Thesis, Univ. of Pittsburgh, Pittsburgh, Pennsylvania (1982).
- Kamath, V.A., Godbole, S.P., Collett, T.S. and Ostermann, R.D.: "Evaluation of Stability of Gas Hydrates in Northern Alaska", Cold Regions Science and Technology, in press (1987).
- Keller, H.H., Couch, E.J., and Berry, P.M.: "Temperature Distribution in Circulating Mud Columns", Soc. Pet. Eng. J., pp. 22-30 (Feb. 1973).
- Kobayashi, R. and Katz, D.L.: "Metastable Equilibrium in the Dew Point Determination of Natural Gases in Hydrate Region", Petroleum Transactions of AIME, Technical Note (294):262 (1955).
- Marshall, D.W. and Bentzen, R.G.: "A Computer Model to Determine the Temperature Distributions in a Wellbore", Journ. Can. Pet. Tech., pp. 63-75 (Jan.-Feb., 1982).

McCloed, H.O. Jr., and Campbell, J.M.: "Natural Gas Hydrates at Pressures to 10,000 Psia", Trans. AIME, 222, p 590 (1961).

Roadifer, R.D., Godbole, S.P. and Kamath, V.A.: "Thermal Model for Establishing Guidelines for Drilling in the Arctic in the Presence of Hydrates", SPE Paper 16361, presented at the SPE California Regional meeting held in Ventura, CA, April 8-10, 1987.

Roadifer, R.D., Godbole, S.P. and Kamath, V.A.: "Estimation of Parameters for Drilling in Arctic and Offshore Environments in the Presence of Hydrates", SPE Paper 16671, paper to be presented at the SPE 62nd Annual Technical Conference and Exhibition, to be held Sept. 27-30, 1987, in Dallas, TX.

Thompson, M.: "The Prediction of Interpretation of Downhole Mud Temperature While Drilling", SPE Paper 14180, presented at the SPE 60th Annual Technical Conference and Exhibition, Las Vegas, NV, Sept. 22-25, 1985.

Tragesser, A.F., Crawford, P.B. and Crawford, H.R.: "A Method for Calculating Circulating Temperatures", Jour. Pet. Tech., pp. 1507-1512 (Nov. 1967).

Wu, B.J., Robinson, D.B. and Ng, H.G.: Journal of Chemical Thermodynamics, 8 (5):461 (1976).

SECTION IV:

**EXPERIMENTAL STUDY OF UNCONSOLIDATED
GAS HYDRATE CORES**

Prepared By

**V.A. Kamath
S.P. Godbole**

TABLE OF CONTENTS FOR SECTION IV

<u>Sub-Section</u>	<u>Title</u>	<u>Page</u>
1	Objective.....	1
2	Perspective	1
3	Work Performed During First Year	1
4	Experimental Set-Up	2
5	Experimental Techniques	7
	a. Hydrate Formation.....	7
	b. Permeability Measurements	9
6	Preliminary Results	9

EXPERIMENTAL STUDY OF UNCONSOLIDATED GAS HYDRATE CORES

1. Objective:

The experimental research on unconsolidated gas hydrate cores has the following major goals:

- a. Development of experimental techniques to form gas hydrates in the unconsolidated sand cores.
- b. Measurement of permeability of gas through these unconsolidated gas hydrate cores as a function of hydrate saturation.
- c. Study of hydrate formation mechanism.
- d. Study of dissociation of the hydrate cores under various conditions such as depressurization, hot brine and steam injection and measurement of gas production rates.
- e. Study of hydrate dissociation mechanism under above conditions to determine conduction and convection heat transfer and mass transfer phenomena.

2. Perspective:

So far, very few studies have been done on hydrate formation and dissociation in porous media, and no experimental data is available on gas production rates during injection of hot brine, steam, or depressurization methods to dissociate hydrates in the porous media. A better understanding of heat and mass transfer effects would be helpful in modelling hydrate production methods so that some of these techniques can be developed commercially. Data gathered in this study will be helpful in evaluating these production methods.

3. Work Performed During The First Year

Although this task had no deliverables for the first year and, according to the work plan provided in the proposal, experimental work was proposed to begin in the

second year, we did start experimental work which is reported in this section.

During the first quarter of the first year, we completed the design of our experimental set up and ordered the equipment components. During the second quarter, we began receiving the equipment components. Late in the second and third quarters we completed the assembly of all the equipment components and necessary piping and fittings. After completion of the experimental set up, we completed preliminary testing of various components, calibration of flow meters, wet test meters, pumps, pressure and temperature measurement devices, and measurement of volumetrics of various components.

In the last quarter, we began the experimental work. Initially, we tested several methods of forming hydrate cores to suit our experimental needs. Then we conducted several runs to measure permeability of gas through hydrate cores as a function of hydrate saturation. Currently, we are in the process of gathering more experimental data on hydrate permeability measurements. The next section provides the experimental set up description, experimental methods employed, and problems encountered during data gathering.

4. Experimental Set-up

Figure 1 shows the schematic diagram of the experimental apparatus for hydrate core formation and dissociation experiments and permeability measurements. Table 1 provides a list of the equipment.

The hydrate core holder is a specially designed unit manufactured by Setra, Inc. The core holder has an internal diameter of 4 inches and a length of 12 inches. It has two flanges on the top and bottom. The core holder has a methanol jacket through which cold methanol is circulated continuously to maintain the core holder at a desired temperature. On one side of the core holder are three pressure taps at 3, 6, and 9 inch distances from the bottom. Pressure transducers

1. Temperature Controller
2. Methanol Bath
3. Refrigeration Cells
4. Heater
5. Digital Temp Indicator
6. Core Holder
- 7,8,9. Pressure Transducers
10. To Methanol Bath
11. Pressure Indicator
12. Gas Flow Meter
13. Gas Cylinder
14. Wet Test Flow Meter
15. Water Tank
16. Gas Water Separator
17. To Vacuum Pump
18. Pressure Gauge
19. Back Pressure Regulator
20. Molten Trap
21. Temperature Control
22. Gas Flow Meter
23. Gas Flow Control
24. Gas Compressor
25. Water Flow Meter
26. Water Pump

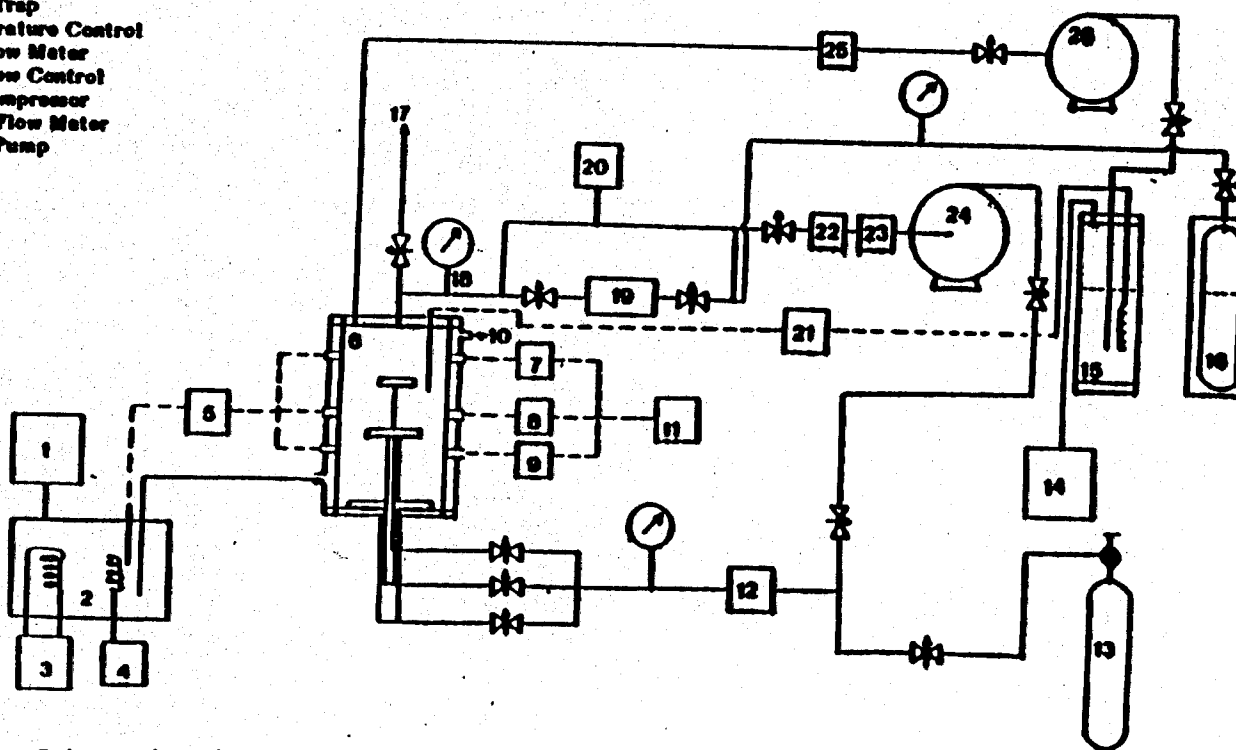


Figure 1: Schematic Diagram of Experimental Setup for Hydrate Core Experiment.

TABLE 1
List of Equipment for Experimental Study of Hydrate Cores

<u>Quantity</u>	<u>Model No</u>	<u>Equipment Received</u>	<u>Company</u>
2	3270	Mass Flow Meter	Cole-Parmer
1	BA-3275-00	Flow Controller	Cole-Parmer
1	—	Sample Cylinder	D.B. Robinson
3	PK-301-2KGV	Pressure Transducers	OMEGA Eng.
1	PRC-3500-P#	Pressure Monitor	OMEGA Eng.
1	BP-1-V	Back Pressure Regulator	TEMCO
1	RTE-4	Bench Top Refrigerated Bath Circulator	Neslab
3	CM	Heise Pressure Gauges	Heise
1	63115	Wet Test Gas Meter	Precision Sc.
1	17-T-40	Water Gas Sample	Jerguson
1	—	Core Holder	Centra
1	3G	Const Metric Pump	LDC Milton Roy
1	AGD-15	Gas Compressor	Haskel
1	1397	Vacuum Pump	Welch
1	AC-523	Air Compressor	National Air
1	651	Resistance Thermometer	OMEGA Eng.
1	DV-6	Vacuum Pump Gauge	Hasting
1	205-002	Flow Meter/Water	Headland

are hooked up at these three pressure ports to monitor pressure drops within the core during permeability experiments. On the opposite side, there are three thermocouple ports through which thermocouples are inserted to measure temperature profiles within the core. The top flange of the core holder has three ports for gas outlet, water inlet and temperature sensor. The bottom flange has one port for gas inlet. With anticipation of plugging of core due to hydrate formation causing no gas flow and increase in inlet pressure, we decided to use a specially designed system for gas inlet. This specially designed gas inlet system consisted of three gas spargers located at three different positions within the core and hooked up to gas inlets through three concentric tubes. This system allowed inlet of gas at three different locations of the core so that if the bottom sparger plugs up due to hydrate formation the top one can allow gas flow. This gas inlet assembly was discontinued in the later experiments due to change in experimental procedures.

Bench top refrigerated bath circulator (Model RTE-4) manufactured by Neslab, Inc., is used for cooling methanol, controlling the temperature of methanol and circulating it through the jacket of the hydrate core holder at desired temperatures. Three pressure transducers (Model #PK-301-2KGV) are hooked to core holder ports at the side and connected to digital pressure monitor (Model #PRC-3500-P3), all manufactured by Omega Engineering, and have a range of 0-2000 psia pressure. All three platinum resistance thermometers are inserted at three temperature ports of the core holder and connected to digital temperture indicator ($\pm 0.1^{\circ}\text{C}$ divisions).

The gas inlet line has a gas flow meter (0-1000 cc/min, Model #3270, Cole Parmer) and a gas flow controller (0-100% range, Model # BA-3275-00, Cole-Parmer, 0.1% flow accuracy). The inlet gas line was passed through a series of coils inserted in the methanol bath for precooling of inlet gas prior to core holder.

The gas outlet line also has a gas flow meter to measure the outlet gas flow during permeability measurements. (In addition, a wet test flow meter was also hooked up to the gas outlet line.)

To achieve continuous gas flow in the core holder without loss of significant amounts of gas, a gas compressor was connected to the gas outlet line. This is a air driven gas compressor (Haskel Model #AGD-15) and is driven by an air compressor (100 psi air supply pressure). The compressed outlet gas is recycled back to the core holder. This compressor and recycling procedure was discontinued in the later experiments due to severe pressure and gas flow fluctuations in the inlet line. Also installed in the inlet and outlet line for gas are the Heise pressure gauges (Model M, 0-2000 psig).

The water inlet line of the core holder is hooked to a constant rate high pressure water pump (0-1.6 lit/min capacity, LDC Milton Roy Co.). This pump is used for injecting hot brine or water in the hydrate core holder during dissociation experiments. The hot water or brine supply to the pump comes from a high pressure vessel termed as hot water or brine tank. In this vessel the brine is heated to a temperature by an immersion heater controlled by a temperature controller such that the sensor inserted into the liquid phase of the core holder senses a constant desired temperature. To determine material balance on gas produced during hydrate dissociation and water injected, a liquid level of the brine (or water) in the tank is measured by a liquid level indicator (Jerguson Gauge). This also acts as a gas water separator for a line that allows the flow of dissociated gas and water from the core holder and is connected to a back pressure regulator and wet test meter to measure gas production rates during dissociation experiments. All system parts could be evacuated independently by a vacuum pump.

The thermocouples, pressure transducers, water pump, methanol bath, wet test meter, gas flow meter, and gas flow controllers were calibrated prior to the

start of the experiments.

5. Experimental Techniques

a. Hydrate Formation:

We tried several methods and variations of hydrate formation. These methods are summarized as follows:

Method 1:

In this method we used a gas sparger system within the core. Initially, 20 mesh Ottawa sand was charged by the core holder and then packed using a vibrator assembly. The porosity was determined and then the core was saturated completely with water. After closing the core holder and evacuating it for 15-20 minutes, the temperature of the core holder was dropped and held at a constant value of 2 to 3°C. Methane at an inlet pressure of 1,000 psi (6.7 MPD) and flow rate of 50-60 cc/min was continuously supplied from the bottom of the core holder. The compressor assembly was also used in this method to recycle the outlet methane gas back to the core holder. In this method we did succeed in the formation of hydrates in the pores of the core and, we also observed in one experiment, plugging of the sparger opening due to hydrate formation. In this case we changed the gas supply to the next sparger to continue the flow. Several problems encountered led us to discontinue this method. One problem was that due to the upward flow of gas, the water from the core was displaced by the gas and large amounts of hydrates also formed on the top (outside of the core) which was undesirable for the experimental measurements. Other problems were that the sparger assembly caused problems of cleaning the core and charging sand and compaction.

Another variation of this method was to remove gas sparger assembly

and injecting gas from the top instead of the bottom. However, this method also was discontinued due to entrainment of water in the lines and in the flow meter which resulted in erroneous gas flow measurements.

Due to problems of water entrainment in the lines, we decided to switch to another variation of this method. In this variation, we installed semipermeable plates on the gas outlet line so that no water can flow through the lines but allow gas to flow through. Although this method was partially successful in not allowing water beyond semi-permeable plates, the problems of material balance were encountered due to large amounts of water that were displaced from the core holder and remained in line between core holder and semipermeable plate. Thus, this method can be successfully used by placing the semipermeable plate within the core holder itself. This will provide all of the water in the core to remain within the core. This variation will be tried later during the next quarter.

Method 2:

In this method, we used finely divided crystal of ice (frost, approximately 400 micron size) instead of saturating the core with water. The sand and frost were thoroughly mixed and compacted. This is the same method as discussed by Kamath (1984). Prior to charging sand and frost, the core holder was cooled to -15°C so that no melting of the frost would take place during charging. It is very essential to maintain the quality of frost to be high (i.e. no wet frost). This method was very successful in terms of hydrate formation rates. Again we tried several variations of this method so that we could make reliable measurements of permeability of the core.

One variation, was to continuously inject gas at a desired rate. This method was discontinued due to problems of pressure and flow fluctuations from the compressor. Instead of recycling the gas we tried a continuous fresh

supply of gas so that pressure and flow fluctuations could be eliminated. This procedure required a large consumption of gas and also posed problems of material balance. We also varied the direction of the gas injection. Instead of upward gas flow we used downward gas flow.

The most economical, as well as successful method, was forming hydrates in batch gas injection process. The procedure was exactly the same as described by Kamath (1984). The only modifications were permeability measurements as described later.

b. Permeability Measurements:

In order to measure permeability of gas through the hydrate core we implemented the following method:

After charging frost and sand, compacting the core and evacuation, the core holder pressure was raised to 600 psia and at constant temperature of 0.5°C. The initial gas permeability when no hydrates are formed was measured by continuously flowing gas from the top at a rate of 400-500 cc/min for 15 minutes. During these 15 minutes of gas flow, at every minute, the gas flow rate and pressure drops were measured. From these readings, initial core permeability was determined using Darcy's law. Precautions were taken to make sure the gas flows were within the range for which Darcy's law is valid. After that, the gas flow was stopped and systems pressure was raised to 700 psia. Hydrates were allowed to form as observed by pressure within the core dropping with time. When pressure dropped to 600 psia, the amount of conversion of frost to hydrates was determined.

6. Preliminary Results

We observed significant increases in pressure drops and decreases in permeability due to hydrate formation. Typically, starting with 700 MD

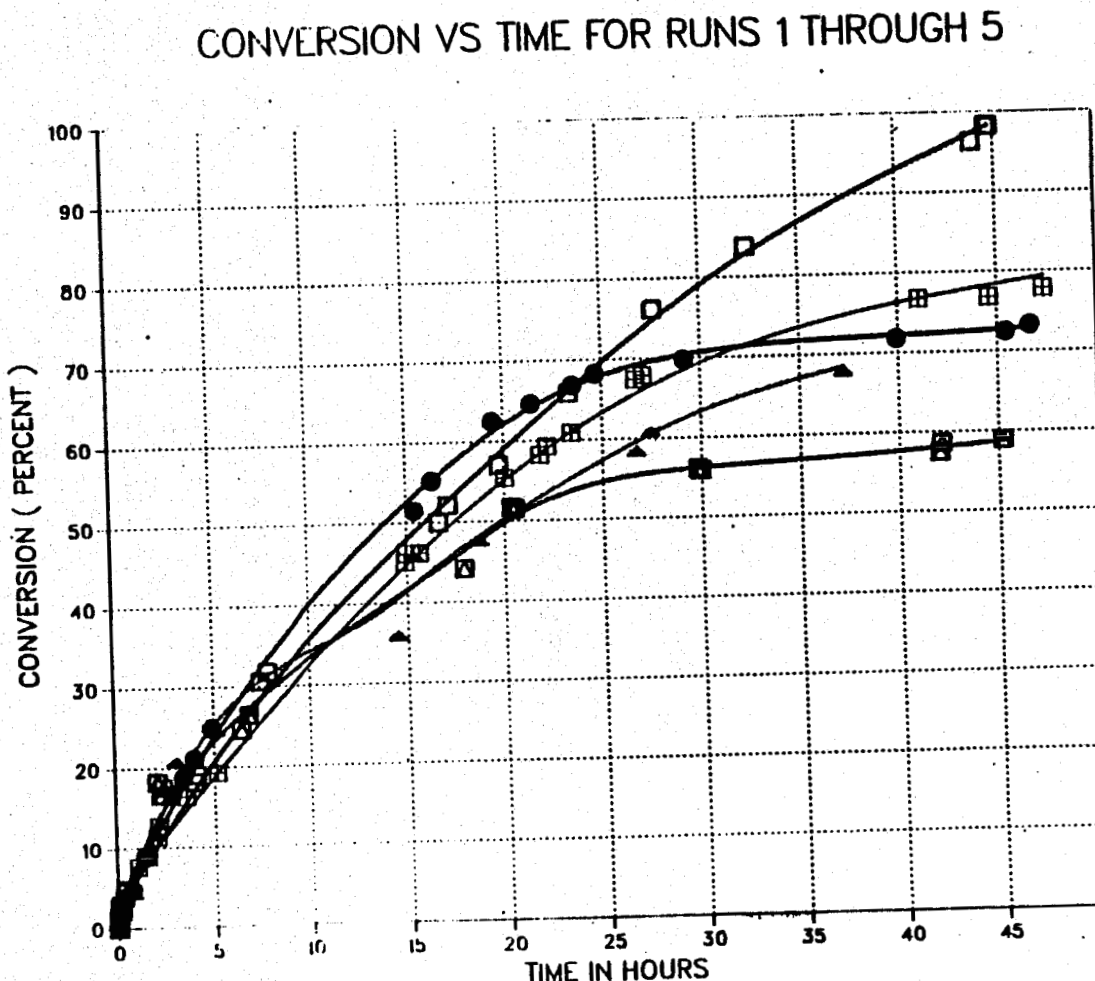
initial core permeability at 70% hydrate saturation the permeability dropped to 3-4 MD.

Tables 2 and 6 give the experimental conditions of our experiments. Figure 2 shows various runs for which hydrate conversion (or saturation) versus time is plotted. Figure 3 shows permeability of the core versus hydrate saturation.

Note that, although the initial permeability varies from run to run depending upon the properties of the core, the ratio of core permeability at any hydrate saturation to initial permeability can be correlated as a function of hydrate saturation.

Currently, we are in the process of collecting more data and obtaining more reliable, reproducibility of the data.

Figure 2: Hydrate Saturation (Conversion) in the Core
Versus Time for Various Runs



Legend

- RUN #1
- RUN #2
- RUN #3
- RUN #4
- ▲ RUN #5

CORE PERMEABILITY VS PERCENT HYDRATES

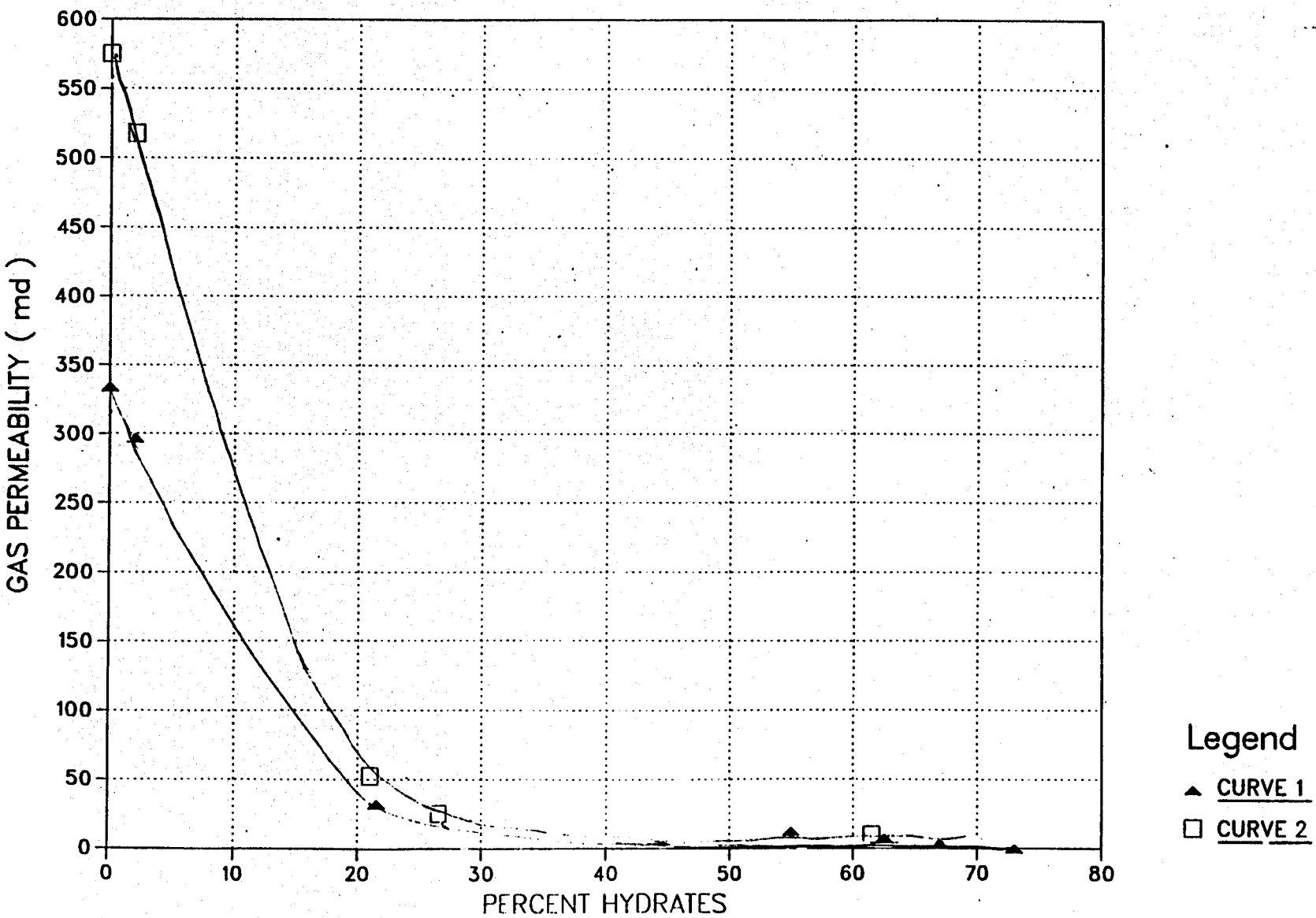


Figure 3: Gas Permeability in the Core as a Function of Hydrate Saturation in the Core

RESULTS OF METHANE HYDRATE FORMATION RUNS

METHANE HYDRATE FORMATION RUN # 1
 DATE RUN STARTED: 10-19-1987
 DATE RUN ENDED: 10-22-1987
 GRAMS OF H₂O = 819.400
 GRAMS OF SAND = 831.800
 HEIGHT OF THE CORE = 22.35CM.
 ROOM TEMPERATURE = 21.0000DEG.C
 TEMP. OF GAS LEAVING WET TEST METER = 16.7000DEG.C
 BAROMETRIC PRESSURE = 742.800MM.HG
 VAP.PRESSURE OF WATER AT TWTM = 14.100MM.HG
 ICE TO SAND VOL.RATIO = 2.782
 ICE TO SAND MASS RATIO = 0.985
 PERCENTAGE voids IN THE CORE = 32.962
 GMOL.METHANE FOR 100 PERCENT CONVERSION = 7.909881

HYDRATE FORMATION RUN INPUT DATA

TIME (HR)	P1 (PSIA)	P3 (PSIA)	PL (PSIA)	PM (PSIA)	PR (PSIA)	T1RTD (DEG.C)	T2RTD (DEG.C)	FIREAD	VWTH (LIT)
0.00	593.00	594.00	595.00	593.00	594.00	-0.20	-0.80	0.00	0.00
0.17	586.00	584.00	587.00	585.00	586.00	-0.20	-0.80	0.00	0.00
0.18	586.00	584.00	587.00	585.00	586.00	-0.20	-0.80	18.60	0.33
0.20	582.00	582.00	584.00	582.00	583.00	-0.20	-0.80	17.30	0.66
0.22	580.00	578.00	581.00	579.00	581.00	-0.20	-0.80	16.70	0.98
0.27	575.00	572.00	576.00	574.00	575.00	-0.40	-1.10	36.70	2.30
0.30	573.00	568.00	574.00	572.00	573.00	-0.40	-1.10	36.50	2.79
0.33	572.00	566.00	572.00	570.00	571.00	-0.40	-1.10	0.00	3.42
0.42	794.00	792.00	796.00	793.00	795.00	-0.30	-0.80	0.00	0.00
0.75	767.00	764.00	770.00	766.00	768.00	-0.30	-0.80	0.00	0.00
0.92	756.00	751.00	760.00	757.00	759.00	-0.30	-0.80	0.00	0.00
1.42	718.00	709.00	721.00	717.00	719.00	0.30	-0.90	0.00	0.00
2.83	612.00	614.00	645.00	655.00	616.00	0.40	-1.00	0.00	0.00
3.42	586.00	586.00	645.00	654.00	583.00	0.40	-1.00	0.00	8.15
4.00	554.00	556.00	642.00	650.00	653.00	0.40	-1.00	17.10	9.20
4.03	554.00	556.00	642.00	650.00	653.00	0.40	-1.00	17.50	11.30
4.10	530.00	530.00	642.00	612.00	632.00	0.40	-1.00	17.50	12.40
4.13	524.00	524.00	642.00	592.00	631.00	0.30	-0.90	0.00	14.30
4.33	610.00	585.00	642.00	576.00	644.00	0.30	-0.90	0.00	0.00
4.42	783.00	783.00	783.00	783.00	783.00	0.30	-0.90	0.00	0.00
4.92	746.00	746.00	744.00	614.00	741.00	-0.10	0.40	0.00	0.00
12.58	398.00	400.00	401.00	460.00	399.00	0.50	0.00	0.00	14.10
15.42	401.00	402.00	404.00	461.00	400.00	4.50	4.40	0.00	31.60
15.50	602.00	603.00	603.00	462.00	600.00	3.00	3.80	36.00	31.60
15.92	570.00	572.00	502.00	449.00	569.00	3.20	3.70	36.00	32.25
15.95	566.00	568.00	497.00	447.00	564.00	2.80	3.20	36.00	32.80
15.99	564.00	565.00	495.00	446.00	562.00	3.00	3.60	36.00	33.03
16.02	563.00	564.00	494.00	445.00	560.00	4.40	9.10	0.00	33.40
16.33	975.00	375.00	570.00	459.00	306.00	2.70	2.50	0.00	0.00
18.42	986.00	886.00	919.00	533.00	796.00	0.70	1.20	0.00	0.00
19.17	968.00	968.00	817.00	483.00	765.00	-0.40	0.40	0.00	36.81
19.45	602.00	602.00	603.00	456.00	580.00	-0.70	-0.10	34.50	38.65
19.58	596.00	596.00	598.00	450.00	556.00	-0.20	0.10	31.00	39.65
19.61	594.00	593.00	595.00	448.00	546.00	-0.50	-0.20	27.00	40.60
19.65	591.00	591.00	593.00	446.00	541.00	-0.40	0.10	41.00	41.50
19.69	588.00	589.00	590.00	445.00	535.00	0.10	-0.20	0.00	0.00
19.92	702.00	702.00	703.00	440.00	532.00	-0.20	-0.40	0.00	0.00
21.42	681.00	682.00	683.00	509.00	533.00	-0.40	-0.70	0.00	0.00
22.58	670.00	671.00	675.00	509.00	558.00	0.00	-0.20	0.00	0.00
23.33	663.00	664.00	667.00	509.00	556.00	1.10	-0.30	0.00	9.50
23.42	600.00	600.00	603.00	509.00	555.00	-0.30	-0.80	29.70	10.50
23.50	591.00	592.00	594.00	509.00	554.00	-0.30	-0.40	38.90	11.22
23.53	589.00	590.00	593.00	509.00	554.00	-0.50	-0.60	35.10	11.32
23.57	590.00	592.00	593.00	509.00	553.00	-0.20	-0.30	34.00	12.22
23.60	592.00	594.00	597.00	509.00	551.00	-0.50	-0.60	33.00	12.42
23.63	595.00	596.00	600.00	509.00	550.00	-0.60	-0.30	0.00	0.00
23.67	766.00	768.00	771.00	509.00	550.00	-0.20	-0.30	0.00	0.00
24.67	754.00	755.00	758.00	508.00	548.00	0.40	0.10	0.00	0.00
25.92	747.00	748.00	752.00	508.00	543.00	0.00	-0.30	0.00	0.00
27.42	740.00	741.00	743.00	507.00	519.00	-0.10	-0.40	0.00	0.00
29.17	734.00	734.00	737.00	507.00	504.00	-0.20	-0.60	0.00	0.00
39.92	707.00	708.00	711.00	505.00	472.00	-0.20	-0.60	0.00	0.00
45.42	698.00	700.00	701.00	505.00	499.00	-0.20	-0.60	0.00	0.00
45.83	740.00	740.00	742.00	505.00	503.00	-0.60	-0.70	0.00	19.18
46.33	599.00	600.00	603.00	505.00	514.00	-0.30	-0.40	16.50	21.70
46.55	585.00	586.00	588.00	505.00	505.00	-0.40	-0.70	15.60	22.16
46.58	584.00	585.00	587.00	505.00	504.00	-0.40	-0.70	16.60	22.75
46.62	582.00	584.00	586.00	505.00	504.00	0.00	0.30	0.00	22.79

RESULTS OF HYDRATE RUN

TIME (HR)	PBAR (PSIA)	TBAR (DEG.C)	QBAR (CC/MIN)	CONV (%)	TIME	GMOLE	CMOLE	CMOLEIN	CMOLELT	CMOLELT
0.000	593.500	0.000	0.000	0.000	0.0000	1.4300	3.6200	0.0000	0.0000	0.0000
0.167	585.000	0.000	0.000	0.655	0.1670	1.5200	3.5451	0.0000	0.0000	0.0014
0.183	585.000	0.000	207.593	0.772	0.1830	1.5292	3.5651	0.0231	0.0139	0.0611
0.200	582.000	0.000	198.532	1.100	0.2000	3.6368	3.5498	0.0215	0.0139	0.0573
0.217	579.000	0.000	191.988	1.423	0.2170	3.6441	3.5315	0.0208	0.0135	0.1126
0.267	573.500	-0.250	567.605	1.680	0.2670	3.6341	3.5012	0.0457	0.0557	0.1329
0.300	570.500	-0.250	370.151	2.225	0.3000	3.6588	3.4829	0.0454	0.0207	0.1760
0.333	569.000	-0.250	403.221	2.579	0.3330	3.6777	3.4737	0.0454	0.0266	0.2040
0.417	793.000	-0.250	0.000	2.579	0.4170	5.0452	4.8412	1.3675	0.0000	0.2040
0.750	765.500	-0.050	0.000	4.744	0.7500	5.0452	4.6699	0.0000	0.0000	0.3753
0.917	753.500	-0.050	0.000	5.670	0.9170	5.0452	4.5967	0.0000	0.0000	0.4485
1.417	713.500	-0.050	0.000	8.755	1.4170	5.0452	4.3527	0.0000	0.0000	0.6925
2.833	613.000	0.200	0.000	16.549	2.8330	5.0452	3.7362	0.0000	0.0000	1.3090
3.417	586.000	0.200	0.000	18.630	3.4170	5.0452	3.5716	0.0000	0.0000	1.4736
4.000	555.000	0.200	0.000	21.018	4.0000	5.0452	3.3827	0.0000	0.0000	1.6625
4.033	555.000	0.200	367.214	20.728	4.0330	5.0222	3.3827	0.0213	0.0443	1.6395
4.100	530.000	0.200	618.030	21.810	4.1000	4.9554	3.2303	0.0218	0.0885	1.7251
4.133	524.000	0.200	381.813	21.961	4.1330	4.9308	3.1937	0.0218	0.0464	1.7371
4.333	597.500	0.200	0.000	21.961	4.3330	5.3788	3.6417	0.4480	0.0000	1.7371
4.417	783.000	0.200	0.000	21.961	4.4170	6.5094	4.7723	1.1306	0.0000	1.7371
4.917	746.000	0.200	0.000	24.812	4.9170	6.5094	4.5468	0.0000	0.0000	1.9626
12.580	399.000	0.650	0.000	51.600	12.5800	6.5094	2.4279	0.0000	0.0000	4.0815
15.420	401.500	0.750	0.000	51.419	15.4200	6.5094	2.4422	0.0000	0.0000	51.4194
15.500	602.500	4.950	0.000	51.419	15.5000	7.6767	3.6094	1.1673	0.0000	4.0672
15.920	571.000	3.900	0.000	53.641	15.9200	7.6767	3.4337	0.0000	0.0000	4.2430
15.950	567.000	3.950	404.461	54.173	15.9500	7.6940	3.4090	0.0448	0.0274	4.2850
15.980	564.500	3.500	380.839	54.566	15.9800	7.7156	3.3995	0.0448	0.0232	4.3161
16.020	563.500	3.800	305.250	55.132	16.0200	7.7507	3.3998	0.0448	0.0097	4.3609
16.330	975.000	7.250	0.000	55.132	16.3300	10.1540	5.7931	2.4033	0.0000	4.3609
19.420	986.000	3.100	0.000	60.918	18.4200	10.1540	5.3434	0.0000	0.0000	4.8106
19.170	868.000	1.450	0.000	61.793	19.1700	10.1540	5.2663	0.0000	0.0000	4.8877
19.450	602.000	0.500	0.000	62.414	19.4500	8.6020	3.6651	0.0000	1.5520	4.9369
19.530	596.000	0.118	475.103	62.371	19.5800	8.5673	3.6339	0.0429	0.0776	4.9335
19.610	591.000	0.450	452.156	62.577	19.6100	8.5637	3.6140	0.0386	0.0422	4.9497
19.650	591.000	0.100	412.396	62.629	19.6500	8.5573	3.6034	0.0336	0.0401	4.9539
19.680	591.000	0.350	195.365	63.028	19.6900	8.5703	3.5849	0.0510	0.0379	4.9855
3.320	701.000	0.450	0.000	43.028	19.9200	9.2602	4.2747	0.6898	0.0000	4.9855
3.320	701.000	0.450	0.000	44.559	21.4200	9.2602	4.1537	0.0000	0.0000	5.1065
3.320	701.000	0.450	0.000	45.359	22.5800	9.2602	4.0904	0.0000	0.0000	5.1698
3.320	701.000	0.450	0.000	45.451	23.1300	9.2602	4.0410	0.0000	0.0000	5.2192
3.320	701.000	0.450	0.000	45.451	23.4200	8.9019	3.6476	0.0000	0.3584	5.2542
3.320	701.000	0.450	0.000	45.734	23.5000	8.8532	3.6117	0.0357	0.0841	5.2414
3.320	701.000	0.450	0.000	45.733	23.5300	8.8712	3.5936	0.0484	0.0304	5.2776
3.320	701.000	0.450	0.000	45.405	23.5700	8.8896	3.6054	0.0437	0.0253	5.2842
3.320	701.000	0.450	0.000	45.357	23.6000	8.9150	3.6136	0.0423	0.0169	5.3014
3.320	701.000	0.450	0.000	45.351	23.6300	8.9476	3.6328	0.0411	0.0084	5.3148
3.320	701.000	0.450	0.000	45.392	23.6700	9.9870	4.6722	1.0394	0.0000	5.3148
3.320	701.000	0.450	0.000	45.421	24.6700	9.9870	4.5978	0.0000	0.0000	5.3893
3.320	701.000	0.450	0.000	45.477	25.9200	9.9870	4.5468	0.0000	0.0000	5.4402
3.320	701.000	0.450	0.000	45.377	27.4200	9.9870	4.5108	0.0000	0.0000	5.4762
3.320	701.000	0.450	0.000	45.771	29.1700	9.9870	4.4728	0.0000	0.0000	5.5142
3.320	701.000	0.450	0.000	45.771	39.9200	9.9870	4.3137	0.0000	0.0000	5.6733
3.320	701.000	0.450	0.000	45.374	45.4200	9.9870	4.2619	0.0000	0.0000	5.7251
3.320	701.000	0.450	0.000	45.374	45.8300	10.2370	4.5119	0.2500	0.0000	5.7251
3.320	701.000	0.450	0.000	45.374	46.3300	9.4283	3.6586	0.0000	0.8087	5.7697
3.320	701.000	0.450	0.000	45.371	46.5500	9.3426	3.5692	0.0205	0.1062	5.7734
3.320	701.000	0.450	0.000	45.371	46.5800	9.3426	3.5657	0.0194	0.0194	5.7769
3.320	701.000	0.450	0.000	45.371	46.6200	9.3384	3.5566	0.0207	0.0249	5.7818
3.320	701.000	0.450	0.000	45.371	46.6500	9.3367	3.5475	0.0000	0.0017	5.7892

Attachment 2

SECTION 4

RESULTS OF HYDRAULIC RUN

TIME (HR)	PBAR (PSIA)	TBAR (DEG.C)	QBAR (CC/XHR)	CONV (%)	TYPE	CHD/LD	JNDL/D	JNDL/CD	WV1	WV2
0.000	593.500	0.000	0.000	0.000	1.1000	1.1000	1.1000	1.1000	0.0000	0.0000
0.167	585.000	0.000	0.000	0.655	0.1670	1.4200	1.1161	0.0000	0.3000	1.0000
0.333	585.000	0.000	207.512	0.772	0.1830	1.4332	1.1491	0.0231	1.2119	1.0411
0.500	582.000	0.000	198.512	1.100	0.2000	1.6368	1.5448	0.0211	0.0179	0.4472
0.667	579.000	0.000	191.628	1.423	0.2170	1.6641	1.5915	0.0208	0.0175	0.1194
0.833	573.500	-0.250	867.605	1.680	0.2470	2.6341	1.8012	0.0437	0.0257	0.1121
0.100	570.000	-0.250	370.151	2.325	0.3000	3.6388	2.4829	0.0434	0.0207	0.1760
0.183	569.000	-0.250	401.221	2.379	0.3320	3.6777	2.4737	0.0434	0.0264	0.2040
0.317	791.000	-0.250	0.000	2.378	0.4170	5.0452	4.8412	1.3573	0.0000	0.2040
0.750	745.300	-0.050	0.000	4.744	0.7100	5.0452	4.6419	0.0000	0.0000	0.3753
0.917	733.500	-0.050	0.000	5.670	0.9170	5.0452	4.8367	0.0000	0.0000	0.4483
1.117	713.300	-0.050	0.000	5.785	1.4170	5.0452	4.3527	0.0000	0.0000	0.8925
1.313	613.000	0.200	0.000	16.649	2.8130	5.0452	5.7181	0.0000	0.0000	1.3090
1.617	586.000	0.200	0.000	18.630	3.4170	5.0452	5.8716	0.0000	0.0000	1.4736
2.000	555.000	0.200	0.000	21.012	4.0000	5.0452	5.8827	0.0000	0.0000	1.6625
2.400	553.000	0.200	367.314	20.728	4.0320	5.0222	5.1827	0.0211	0.0443	1.6395
2.800	530.000	0.200	618.030	21.810	4.1000	4.9334	5.2303	0.0218	0.0883	1.7251
3.133	524.000	0.200	381.813	21.981	4.1330	4.9308	5.1937	0.0218	0.0464	1.7271
3.333	527.500	0.200	0.000	21.981	4.2320	5.3788	5.6417	0.4480	0.0000	1.7271
4.417	783.000	0.200	0.000	21.981	4.3170	5.3014	5.7723	1.1305	0.0000	1.7271
4.917	746.000	0.200	0.000	34.818	4.9170	4.1094	4.5464	0.0000	0.0000	1.8626
12.380	399.000	0.650	0.000	51.600	12.1800	6.5094	2.4278	0.0000	0.0000	4.0815
15.420	401.500	0.750	0.000	51.415	15.4200	6.5094	2.4472	0.0000	0.0000	4.0672
18.500	602.500	4.850	0.000	51.415	15.8000	7.1767	1.6094	1.1673	0.0000	4.0672
18.920	571.000	3.200	0.000	51.641	15.9200	7.6767	1.4217	0.0000	0.0000	4.2430
19.930	567.000	1.850	404.161	54.173	15.9500	7.6940	3.4030	0.0448	0.0274	4.2330
19.980	564.500	3.800	380.839	54.166	15.9800	7.7186	3.3995	0.0448	0.0232	4.3161
16.020	561.500	1.800	303.250	51.132	16.0200	7.7307	3.3995	0.0448	0.0097	4.3609
14.310	578.000	7.250	0.000	53.102	16.3300	10.1540	5.7911	1.4033	0.0000	4.3609
14.420	494.000	2.100	0.000	50.118	18.4200	10.1540	5.3614	0.0000	0.0000	4.8106
19.170	168.000	1.450	0.000	51.793	19.1700	10.1540	5.2663	0.0000	0.0000	4.8877
19.420	402.172	0.300	0.000	43.414	19.4500	8.6020	3.6621	0.0000	1.5320	4.9369
19.530	398.000	1.111	479.103	42.371	19.5800	8.5673	3.6333	0.0419	0.0776	4.9335
19.540	511.100	0.450	451.144	42.377	19.4100	8.1567	3.6140	0.0386	0.0422	4.9497
19.540	141.000	2.100	412.149	42.324	19.4500	8.5973	3.6034	0.0336	0.0401	4.9339
19.540	0.140	451.173	43.028	19.9900	8.5703	3.1849	0.0510	0.0379	4.9355	41.0251
19.540	0.140	0.000	43.028	19.9200	9.2602	4.2747	0.6838	0.0000	4.9355	43.0251
19.540	0.140	0.000	44.359	21.4200	9.2602	4.1817	0.0000	0.0000	5.1065	44.1385
19.540	0.140	0.000	44.359	22.5800	9.2802	4.0904	0.0000	0.0000	5.1695	45.1555
19.540	0.140	0.000	45.141	21.1100	9.1402	4.0410	0.0000	0.0000	5.2192	45.1419
19.540	0.140	0.000	45.141	23.4200	9.3018	3.0479	2.0000	0.3384	5.2562	46.4257
19.540	0.140	0.000	45.141	23.5000	9.3332	3.0117	0.0157	0.0441	5.3414	46.3862
19.540	0.140	0.000	45.141	23.5300	9.3712	3.1936	0.0484	0.0304	5.2776	46.7717
19.540	0.140	0.000	45.141	23.5700	9.3894	3.0954	0.0417	0.0351	5.2842	46.9050
19.540	0.140	0.000	45.141	23.6000	9.3136	3.6136	0.0423	0.0169	5.3014	47.0285
19.540	0.140	0.000	45.141	23.6100	9.3476	3.6328	0.0411	0.0064	5.3148	47.1919
19.540	0.140	0.000	45.141	23.6700	9.3570	4.6722	1.0394	0.0000	5.3148	47.1919
19.540	0.140	0.000	45.141	24.6700	9.1870	4.5978	0.0000	0.0000	5.3893	48.1333
19.540	0.140	0.000	45.141	25.3200	9.3870	4.5464	0.0000	0.0000	5.4403	48.7777
19.540	0.140	0.000	45.141	27.4200	9.3870	4.5108	0.0000	0.0000	5.4762	49.2327
19.540	0.140	0.000	45.141	29.1700	9.3870	4.4728	0.0000	0.0000	5.5162	49.7126
19.540	0.140	0.000	45.141	29.9200	9.3870	4.3137	0.0000	0.0000	5.4723	51.7243
19.540	0.140	0.000	45.141	43.4200	9.3870	4.2619	0.0000	0.0000	5.7251	52.3795
19.540	0.140	0.000	45.141	45.8300	10.2372	4.5119	0.2500	0.0000	5.7251	52.3795
19.540	0.140	0.000	45.141	46.3200	9.4233	3.6586	0.0000	0.0000	5.7457	52.4436
19.540	0.140	0.000	45.141	46.3500	9.3426	3.5692	0.0203	0.1062	5.7734	52.4895
19.540	0.140	0.000	45.141	46.3800	9.3436	3.5697	0.0184	0.0184	5.7769	52.6238
19.540	0.140	0.000	45.141	46.4200	9.3384	3.5366	0.0207	0.0249	5.7818	52.9461
19.540	0.140	0.000	45.141	46.4500	9.3367	3.5473	0.0000	0.0017	5.7822	53.1897

METHANE HYDRATE FORMATION RUN # 2
 DATE RUN STARTED: 10-25-1987
 DATE RUN ENDED: 10-27-1987
 GRAMS OF H₂O = 861.100
 GRAMS OF SAND = 881.000
 HEIGHT OF THE CORE = 29.21CM.
 ROOM TEMPERATURE = 20.8000DEG.C
 TEMP. OF GAS LEAVING WET TEST METER = 16.8000DEG.C
 BAROMETRIC PRESSURE = 743.300MM.HG
 VAP.PRESSURE OF WATER AT TWTH = 14.071MM.HG
 ICE TO SAND VOL.RATIO = 2.761
 ICE TO SAND MASS RATIO = 0.977
 PERCENTAGE VOIDS IN THE CORE = 45.983
 CHOL.METHANE FOR 100 PERCENT CONVERSION = 8.312421
 HYDRATE FORMATION RUN INPUT DATA

TIME (HR)	P1 (PSIA)	P3 (PSIA)	P _L (PSIA)	P _M (PSIA)	P _R (PSIA)	T _{IRTD} (DEG.C)	T _{ZRTD} (DEG.C)	FIREAD	VWTM (LIT)
0.00	750.00	750.00	749.00	750.00	741.00	-0.60	-0.60	0.00	0.00
0.03	738.00	737.00	737.00	735.00	730.00	-0.60	-0.60	3.50	0.62
0.07	727.00	726.00	725.00	727.00	720.00	-0.60	-0.60	4.10	1.40
0.10	718.00	718.00	715.00	716.00	709.00	-0.50	-0.60	4.50	2.00
0.17	690.00	690.00	689.00	690.00	688.00	-0.50	-0.60	7.80	5.20
0.18	678.00	678.00	678.00	676.00	678.00	-0.50	-0.60	6.90	6.31
0.35	668.00	668.00	667.00	668.00	665.00	-0.50	-0.60	6.80	7.39
2.07	438.00	438.00	435.00	437.00	438.00	-0.40	-0.30	0.00	0.00
2.12	610.00	610.00	609.00	611.00	467.00	-0.40	-0.30	0.00	7.39
2.19	625.00	625.00	626.00	628.00	526.00	-0.40	-0.30	4.10	8.72
2.22	623.00	623.00	623.00	625.00	539.00	-0.40	-0.30	3.80	9.06
2.29	622.00	622.00	619.00	621.00	538.00	-0.40	-0.30	3.70	9.41
2.32	597.00	597.00	595.00	597.00	560.00	-0.40	-0.30	11.60	12.54
2.34	581.00	581.00	580.00	583.00	561.00	-0.40	-0.30	10.90	14.10
2.36	569.00	569.00	567.00	568.00	561.00	-0.40	-0.30	9.80	15.72
2.39	660.00	660.00	661.00	663.00	571.00	-0.40	-0.30	0.00	16.11
6.39	556.00	556.00	445.00	431.00	441.00	-0.20	-0.60	0.00	16.11
6.41	543.00	543.00	461.00	437.00	446.00	-0.20	-0.60	5.90	17.34
6.44	532.00	543.00	468.00	440.00	450.00	-0.20	-0.60	5.60	18.30
6.51	524.00	524.00	471.00	442.00	452.00	-0.20	-0.60	5.50	19.14
6.52	508.00	508.00	475.00	445.00	455.00	-0.20	-0.60	14.40	21.10
6.56	480.00	480.00	474.00	445.00	455.00	-0.20	-0.60	17.60	24.20
6.79	650.00	650.00	543.00	492.00	519.00	-0.20	-0.60	0.00	0.00
17.90	392.00	393.00	390.00	407.00	392.00	0.10	0.20	0.00	0.00
18.00	696.00	697.00	695.00	421.00	572.00	6.80	5.90	0.00	0.00
20.25	576.00	575.00	562.00	520.00	525.00	3.00	1.10	0.00	24.20
20.36	558.00	558.00	562.00	519.00	519.00	2.30	0.70	6.00	26.41
20.39	554.00	555.00	562.00	519.00	518.00	2.30	0.70	6.00	27.22
20.43	550.00	551.00	562.00	519.00	517.00	2.30	0.70	6.00	28.35
20.50	549.00	549.00	562.00	518.00	516.00	2.30	0.70	0.00	0.00
20.68	792.00	792.00	589.00	516.00	583.00	2.70	1.20	0.00	0.00
29.80	718.00	718.00	662.00	469.00	706.00	-0.40	-0.70	0.00	28.50
29.83	714.00	713.00	662.00	469.00	706.00	-0.40	-0.70	6.00	30.10
29.87	704.00	703.00	662.00	469.00	706.00	-0.40	-0.70	6.10	31.72
29.90	696.00	696.00	662.00	469.00	706.00	-0.40	-0.70	5.90	32.99
29.95	692.00	692.00	662.00	469.00	706.00	-0.40	-0.70	0.00	0.00
42.03	669.00	670.00	653.00	466.00	479.00	-0.50	-0.70	0.00	0.00
46.03	664.00	665.00	652.00	466.00	679.00	-0.70	-0.90	0.00	32.99
42.05	650.00	652.00	652.00	466.00	679.00	-1.50	-1.40	27.90	34.94
42.08	647.00	648.00	652.00	466.00	679.00	-0.30	-1.00	28.80	35.73
42.12	645.00	645.00	652.00	466.00	679.00	-0.50	-0.80	30.00	36.62
45.20	600.00	600.00	652.00	466.00	679.00	-0.50	-0.80	0.00	42.12

RESULTS OF HYDRATE RUN

TIME (HR)	PBAR (PSIA)	TBAR (DEG.C)	QBAR (CC/MIN)	CONV (%)	TIME	GMOL0	GMOLG	GMOLIN	GMOLOUT	GMOLH	CONV
0.000	750.000	-0.100	0.000	0.000	0.0000	4.2788	4.2788	0.0000	0.0000	0.0000	0.0000
0.033	737.500	-0.100	173.693	0.602	0.0330	4.2575	4.2075	0.0049	0.0262	0.0500	0.6017
0.066	726.500	-0.100	212.896	1.022	0.0660	4.2297	4.1448	0.0051	0.0329	0.0850	1.0222
0.099	718.000	-0.050	173.149	1.378	0.0990	4.2100	4.0955	0.0056	0.0253	0.1145	1.3775
0.132	690.000	-0.050	810.547	1.792	0.1357	4.0848	3.9358	0.0097	0.1350	0.1490	1.7919
0.166	678.000	-0.050	310.393	2.155	0.1824	4.0465	3.8673	0.0086	0.0468	0.1792	2.1554
0.199	668.000	-0.050	302.607	2.395	0.3500	4.0094	3.8103	0.0085	0.0456	0.1991	2.3954
2.070	438.000	0.150	0.000	18.200	2.0700	4.0094	2.4965	0.0000	0.0000	1.5129	18.2002
2.120	610.000	0.150	0.000	18.200	2.1200	4.9898	3.4769	0.9804	0.0000	1.5129	18.2002
2.190	625.000	0.150	342.865	16.558	2.1900	4.9388	3.5624	0.0051	0.0561	1.3764	16.5581
2.220	623.000	0.150	106.830	16.580	2.2200	4.9292	3.5510	0.0047	0.0143	1.3782	16.5796
2.290	622.000	0.150	108.496	16.526	2.2900	4.9190	3.5453	0.0046	0.0148	1.3737	16.5260
2.320	597.000	0.150	820.491	16.826	2.3200	4.8014	3.4028	0.0144	0.1320	1.3986	16.8256
2.340	581.000	0.150	444.611	17.294	2.3400	4.7492	3.3116	0.0136	0.0658	1.4376	17.2943
2.360	569.000	0.150	451.123	17.442	2.3600	4.6931	3.2432	0.0122	0.0683	1.4498	17.4418
2.390	660.000	0.150	0.000	17.442	2.3900	5.2118	3.7619	0.5187	0.0000	1.4498	17.4418
6.390	556.000	0.100	0.000	24.566	6.3900	5.2118	3.1697	0.0000	0.0000	2.0420	24.5662
6.410	543.000	0.100	331.780	24.922	6.4100	5.1672	3.0956	0.0073	0.0519	2.0716	24.9219
6.440	537.500	0.100	265.886	24.896	6.4400	5.1337	3.0642	0.0070	0.0405	2.0694	24.8958
6.510	524.000	0.100	236.832	25.478	6.5100	5.1051	2.9873	0.0068	0.0354	2.1178	25.4778
6.523	508.000	0.100	563.529	25.796	6.5230	5.0404	2.8961	0.0179	0.0827	2.1443	25.7961
6.560	480.000	0.100	855.222	26.407	6.5600	4.9315	2.7364	0.0219	0.1308	2.1950	26.4069
6.790	650.000	0.100	0.000	26.407	6.7900	5.9006	3.7056	0.9692	0.0000	2.1950	26.4069
17.900	392.500	0.650	0.000	44.121	17.9000	5.9006	2.2331	0.0000	0.0000	3.6675	44.1211
18.000	696.500	6.850	0.000	44.121	18.0000	7.5425	3.8750	1.6419	0.0000	3.6675	44.1211
20.250	575.500	2.550	0.000	51.619	20.2500	7.5425	3.2517	0.0000	0.0000	4.2908	51.6189
20.360	558.000	2.000	564.057	51.701	20.3600	7.4568	3.1591	0.0075	0.0932	4.2976	51.7010
20.393	554.500	2.000	233.228	51.618	20.3930	7.4301	3.1393	0.0075	0.0342	4.2907	51.6182
20.430	550.500	2.000	308.846	51.407	20.4300	7.3899	3.1167	0.0075	0.0477	4.2732	51.4070
20.500	549.000	2.000	0.000	51.509	20.5000	7.3539	3.1082	0.0000	0.0000	4.2817	51.5092
20.680	792.000	2.450	0.000	51.509	20.6800	8.7583	4.4766	1.1644	0.0000	4.2817	51.5092
29.800	718.000	-0.050	0.000	56.094	29.8000	8.7583	4.0955	0.0000	0.0000	4.6628	56.0942
29.833	713.500	-0.050	419.910	55.681	29.8330	8.6983	4.0698	0.0075	0.0675	4.6284	55.6809
29.870	703.500	-0.050	425.334	55.636	29.8700	8.6375	4.0128	0.0076	0.0683	4.6247	55.6364
29.900	696.000	-0.050	341.232	55.595	29.9000	8.5913	3.9700	0.0073	0.0536	4.6213	55.5349
29.950	692.000	-0.050	0.000	55.869	29.9500	8.5913	3.9472	0.0000	0.0000	4.6441	55.5694
42.030	669.500	-0.100	0.000	57.405	42.0300	9.5913	3.8196	0.0000	0.0000	4.7717	57.4049
46.030	664.500	-0.300	0.000	57.715	46.0300	9.5913	3.7938	0.0000	0.0000	4.7975	57.7147
42.050	651.000	-0.950	631.630	58.014	42.0500	8.5480	3.7256	0.0347	0.0780	4.8224	58.0140
42.083	647.500	-0.150	411.049	58.365	42.0830	8.5463	3.6947	0.0358	0.0375	4.8515	58.1650
42.120	645.000	-0.150	419.413	58.534	42.1200	8.5461	3.6805	0.0373	0.0375	4.8656	58.5340
45.200	600.000	-0.150	0.000	58.832	45.2000	8.3141	3.4237	0.0000	0.2320	4.8904	58.8323

METHANE HYDRATE FORMATION RUN # 3
 DATE RUN STARTED: 10-29-1987
 DATE RUN ENDED: 10-31-1987
 GRAMS OF H₂O = 726.000
 GRAMS OF SAND = 710.600
 HEIGHT OF THE CORE = 28.60CM.
 ROOM TEMPERATURE = 21.0000DEG.C
 TEMP. OF GAS LEAVING WET TEST METER = 16.5000DEG.C
 BAROMETRIC PRESSURE = 744.300MM.HG
 VAP.PRESSURE OF WATER AT TWTM = 14.070MM.HG
 ICE TO SAND VOL.RATIO = 2.886
 ICE TO SAND MASS RATIO = 1.022
 PERCENTAGE VOIDS IN THE CORE = 54.022
 GMOL.METHANE FOR 100 PERCENT CONVERSION = 7.088261
 HYDRATE FORMATION RUN INPUT DATA

TIME (HR)	P1 (PSIA)	P3 (PSIA)	PL (PSIA)	PN (PSIA)	PR (PSIA)	T1RTD (DEG.C)	T2RTD (DEG.C)	F1READ	VWTH (LIT)
0.00	696.00	696.00	694.00	694.00	696.00	-0.70	-0.50	0.00	0.00
0.17	664.00	664.00	662.00	662.00	664.00	-0.60	-0.50	0.00	0.00
0.33	644.00	644.00	643.00	643.00	645.00	-0.60	-0.50	0.00	1.67
0.37	637.00	637.00	636.00	636.00	636.00	-0.70	-0.80	19.10	2.30
0.40	636.00	636.00	635.00	635.00	636.00	-0.80	-0.90	18.50	2.70
0.43	635.00	635.00	634.00	634.00	636.00	-0.70	-0.40	18.20	2.91
0.45	736.00	735.00	735.00	735.00	737.00	-0.70	-0.50	0.00	0.00
1.07	707.00	706.00	706.00	705.00	707.00	-0.70	-0.50	0.00	0.00
1.57	693.00	692.00	692.00	691.00	693.00	-0.60	-0.30	0.00	0.00
2.07	667.00	666.00	656.00	655.00	655.00	-0.60	-0.40	0.00	2.91
2.10	651.00	651.00	650.00	649.00	672.00	-0.60	-0.50	20.70	4.96
2.14	648.00	648.00	648.00	647.00	672.00	-0.60	-0.50	20.70	5.27
2.17	644.00	644.00	644.00	644.00	672.00	-0.60	-0.50	19.60	5.93
2.20	756.00	754.00	754.00	754.00	698.00	-0.70	-0.80	0.00	0.00
3.59	717.00	716.00	716.00	716.00	717.00	-0.50	-0.40	0.00	0.00
5.17	684.00	684.00	694.00	713.00	686.00	-0.40	-0.70	0.00	0.00
14.92	407.00	404.00	402.00	402.00	402.00	-0.40	-0.70	0.00	5.93
14.95	402.00	404.00	400.00	399.00	400.00	-0.10	-0.30	17.80	6.30
14.98	397.00	397.00	398.00	396.00	397.00	-0.10	-0.30	17.80	6.57
15.02	395.00	395.00	395.00	395.00	395.00	-0.10	-0.30	19.90	7.41
15.65	776.00	776.00	774.00	762.00	657.00	3.30	-0.30	0.00	0.00
20.04	678.00	680.00	678.00	670.00	664.00	3.20	2.60	0.00	0.00
21.85	648.00	640.00	637.00	641.00	492.00	0.30	-1.40	0.00	7.41
21.89	630.00	630.00	627.00	641.00	492.00	0.20	-1.30	19.90	9.39
21.92	623.00	623.00	620.00	641.00	491.00	0.20	-1.30	19.80	10.48
21.95	614.00	614.00	611.00	641.00	491.00	0.20	-1.30	19.70	11.92
21.98	604.00	604.00	603.00	641.00	491.00	0.20	-1.30	19.60	13.51
22.20	752.00	752.00	749.00	640.00	488.00	-0.40	-7.41	0.00	0.00
23.45	743.00	745.00	744.00	717.00	696.00	-0.50	-0.40	0.00	0.00
0.00	676.00	676.00	676.00	708.00	660.00	5.60	2.50	0.00	13.51
26.73	670.00	670.00	668.00	708.00	666.00	5.20	2.50	20.50	16.30
26.77	665.00	665.00	663.00	708.00	661.00	5.10	2.50	17.50	18.30
26.83	661.00	661.00	659.00	708.00	656.00	5.10	2.40	18.20	18.70
26.84	655.00	655.00	657.00	708.00	656.00	5.10	2.40	18.50	19.30
27.08	805.00	804.00	802.00	708.00	657.00	7.20	2.30	0.00	0.00
41.08	701.00	701.00	699.00	659.00	669.00	2.40	2.30	0.00	0.00
44.58	676.00	676.00	675.00	611.00	569.00	-0.70	-2.40	0.00	19.30
44.61	667.00	667.00	664.00	569.00	0.00	-0.60	-2.20	18.82	23.50
44.65	657.00	656.00	654.00	610.00	569.00	-0.70	-2.20	19.40	24.80
44.68	650.00	649.00	649.00	610.00	569.00	-0.70	-2.50	19.80	25.70
47.36	648.00	648.00	646.00	612.00	563.00	-1.60	-2.10	0.00	0.00

RESULTS OF HYDRATE RUN

TIME	GMOLG	GMOLG	GMOLIN	GMOLOUT	GMOLH	CONV	TIME (HR)	PBAR (PSIA)	TBAR (DEG.C)	QBAR (CC/MIN)	CONV (%)
0.0000	4.5135	4.5135	0.0000	0.0000	0.0000	0.0000	0.000	696.000	-0.100	0.000	0.000
0.1670	4.5135	4.3052	0.0000	0.0000	0.2083	-2.9723	0.167	664.000	-0.050	0.000	2.972
0.3330	4.4429	4.1755	0.0000	0.0706	0.2674	3.8151	0.333	644.000	-0.050	0.000	3.815
0.3670	4.4400	4.1331	0.0238	0.0266	0.3069	4.3785	0.367	637.000	-0.250	282.359	4.378
0.3990	4.4461	4.1282	0.0230	0.0169	0.3179	4.5366	0.399	636.000	-0.350	223.695	4.537
0.4320	4.4599	4.1172	0.0226	0.0089	0.3427	4.8902	0.432	635.000	-0.050	176.598	4.890
0.4500	5.1124	4.7696	0.6525	0.0000	0.3427	4.8902	0.450	735.500	-0.100	0.000	4.890
1.0700	5.1124	4.5816	0.0000	0.0000	0.5308	7.5736	1.070	706.500	-0.100	0.000	7.574
1.5700	5.1124	4.4883	0.0000	0.0000	0.6240	8.9042	1.570	692.500	0.050	0.000	8.904
2.0700	5.1124	4.3206	0.0000	0.0000	0.7918	11.2975	2.070	666.500	0.000	0.000	11.297
2.1030	5.0514	4.2209	0.0258	0.0867	0.8305	11.8509	2.103	651.000	-0.050	629.875	11.851
2.1400	5.0641	4.2014	0.0258	0.0131	0.8626	12.3089	2.140	648.000	-0.050	217.711	12.309
2.1700	5.0606	4.1755	0.0244	0.0279	0.8851	12.6287	2.170	644.000	-0.050	292.950	12.629
2.2000	5.7838	4.8398	0.7233	0.0000	0.8851	12.6287	2.200	755.000	-0.250	0.000	12.629
3.5900	5.7838	4.6439	0.0000	0.0000	1.1400	16.2660	3.590	716.500	0.050	0.000	16.266
5.1700	5.7838	4.4349	0.0000	0.0000	1.3490	19.2485	5.170	684.000	-0.050	0.000	19.248
14.9200	5.7838	2.6291	0.0000	0.0000	3.1547	45.0139	14.920	405.500	-0.050	0.000	45.014
14.9500	5.7903	2.6096	0.0221	0.0156	3.1807	45.3857	14.950	403.000	0.300	211.710	45.386
14.9800	5.8011	2.5707	0.0221	0.0114	3.2303	46.0932	14.980	397.000	0.300	188.022	46.093
15.0200	5.7903	2.5578	0.0248	0.0355	3.2325	46.1245	15.020	395.000	0.300	337.679	46.124
15.6500	8.2264	4.9939	2.4361	0.0000	3.2325	46.1245	15.650	776.000	2.000	0.000	46.124
20.0400	8.2264	4.3475	0.0000	0.0000	3.8789	55.3472	20.040	679.000	3.400	0.000	55.347
21.8500	8.2264	4.1496	0.0000	0.0000	4.0768	58.1716	21.850	640.000	-0.050	0.000	58.172
21.8900	8.1674	4.0847	0.0248	0.0837	4.0827	58.2555	21.890	630.000	-0.050	607.717	58.256
21.9200	8.1460	4.0393	0.0246	0.0461	4.1066	58.5970	21.920	623.000	-0.050	396.201	58.597
21.9500	8.1096	3.9810	0.0245	0.0609	4.1286	58.9106	21.950	614.000	-0.050	478.410	58.911
21.9800	8.0668	3.9162	0.0244	0.0672	4.1506	59.2245	21.980	604.000	-0.050	513.245	59.224
22.2000	9.0870	4.9364	1.0202	0.0000	4.1506	59.2245	22.200	752.000	-3.405	0.000	59.224
23.4500	9.0870	4.8221	0.0000	0.0000	4.2649	60.8551	23.450	744.000	0.050	0.000	60.855
0.0000	9.0870	4.3104	0.0000	0.0000	4.7766	68.1569	0.000	676.000	4.550	0.000	68.157
26.7330	8.9945	4.2752	0.0255	0.1180	4.7193	67.1396	26.733	670.000	4.350	803.769	67.140
26.7700	8.9318	4.2441	0.0218	0.0846	4.6877	66.8880	26.770	665.000	4.300	595.727	66.888
26.8300	8.9375	4.2193	0.0226	0.0169	4.7182	67.1232	26.830	661.000	4.250	221.604	67.123
26.8400	8.9351	4.1810	0.0230	0.0254	4.7541	67.9361	26.840	655.000	4.250	271.071	67.836
27.0800	9.8710	5.1168	0.9358	0.0000	4.7541	67.8361	27.080	804.500	5.250	0.000	67.836
41.0800	9.8710	4.4973	0.0000	0.0000	5.3736	76.6759	41.080	701.000	2.850	0.000	76.676
44.5800	9.8710	4.3991	0.0000	0.0000	5.4719	78.0775	44.580	676.000	-1.050	0.000	78.078
44.6100	9.7168	4.3381	0.0234	0.1776	5.3787	76.7476	44.610	667.000	-0.900	1126.054	76.748
44.6500	9.6860	4.2706	0.0241	0.0550	5.4154	77.2709	44.650	656.500	-0.950	443.157	77.271
44.6830	9.6726	4.2274	0.0246	0.0381	5.4451	77.6960	44.683	549.500	-1.100	351.194	77.696
47.3600	9.6726	4.2215	0.0000	0.0000	5.4510	77.7799	47.360	548.000	-1.350	0.000	77.780

METHANE HYDRATE FORMATION RUN # 4
 DATE RUN STARTED: 11- 2-1987
 DATE RUN ENDED: 11- 4-1987
 GRAMS OF H₂O - 719.800
 GRAMS OF SAND - 714.800
 HEIGHT OF THE CORE - 28.44CM.
 ROOM TEMPERATURE - 20.9000DEG.C
 TEMP.OF GAS LEAVING WET TEST METER - 16.5000DEG.C
 BAROMETRIC PRESSURE - 744.400MM.HG
 VAP.PRESSURE OF WATER AT TWTH - 14.078MM.HG
 ICE TO SAND VOL.RATIO - 2.844
 ICE TO SAND MASS RATIO - 1.007
 PERCENTAGE voids in the core - 53.987
 GMOL.METHANE FOR 100 PERCENT CONVERSION - 6.948411
 HYDRATE FORMATION RUN INPUT DATA

TIME (HR)	P1 (PSIA)	P3 (PSIA)	P _L (PSIA)	PW (PSIA)	PR (PSIA)	T1RTD (DEG.C)	T2RTD (DEG.C)	P1READ	VWTM (LIT)
0.00	749.00	747.00	748.00	746.00	748.00	-2.20	-1.60	0.00	0.00
0.03	728.00	726.00	727.00	725.00	727.00	-2.10	-1.10	18.00	1.68
0.07	719.00	718.00	719.00	717.00	719.00	-2.10	-1.00	17.90	2.51
0.10	712.00	711.00	712.00	709.00	711.00	-1.70	-0.80	17.80	3.49
0.13	706.00	705.00	706.00	704.00	706.00	-1.60	-0.70	17.80	4.14
0.23	769.00	768.00	769.00	767.00	770.00	-1.50	-0.70	0.00	4.30
4.02	607.00	607.00	621.00	607.00	608.00	-0.70	-0.30	0.00	4.30
4.05	602.00	601.00	621.00	602.00	601.00	-0.80	-0.50	19.80	5.09
4.08	599.00	598.00	621.00	599.00	599.00	-0.80	-0.30	19.80	5.82
4.11	594.00	593.00	620.00	594.00	594.00	-0.80	-0.60	19.80	6.54
4.15	589.00	589.00	620.00	589.00	589.00	-1.10	-0.50	19.90	7.52
4.21	722.00	721.00	622.00	721.00	721.00	-3.20	-0.50	0.00	0.00
7.41	602.00	602.00	603.00	601.00	689.00	-0.80	-0.70	0.00	7.52
7.45	596.00	596.00	591.00	593.00	689.00	-0.80	-0.50	15.00	9.22
7.48	590.00	590.00	588.00	587.00	689.00	-0.70	-0.30	19.80	10.01
7.55	584.00	582.00	583.00	582.00	689.00	-0.70	-0.50	19.50	10.77
7.58	580.00	579.00	581.00	580.00	688.00	-0.80	-0.30	19.50	11.32
7.80	888.00	886.00	872.00	869.00	756.00	-1.00	-0.80	0.00	0.00
16.63	693.00	694.00	696.00	698.00	769.00	0.50	-0.40	0.00	11.32
17.05	592.00	592.00	597.00	596.00	735.00	0.50	-0.40	0.00	24.13
17.08	587.00	587.00	594.00	593.00	736.00	1.10	-0.40	19.80	25.04
17.12	583.00	583.00	591.00	590.00	735.00	1.00	-0.40	19.60	25.91
17.15	580.00	580.00	588.00	586.00	736.00	1.30	-0.40	19.60	26.60
17.25	754.00	751.00	751.00	753.00	744.00	2.40	-0.30	0.00	0.00
19.75	701.00	700.00	699.00	699.00	732.00	1.40	-0.40	0.00	0.00
23.32	607.00	607.00	607.00	618.00	728.00	0.20	3.10	0.00	26.60
23.35	599.00	599.00	605.00	615.00	727.00	2.20	4.50	20.00	27.72
23.39	594.00	593.00	601.00	611.00	727.00	2.10	4.40	19.90	28.47
23.42	589.00	588.00	595.00	604.00	726.00	2.10	4.30	19.90	29.08
23.45	584.00	583.00	591.00	597.00	726.00	2.50	4.30	19.80	29.93
23.64	750.00	750.00	739.00	749.00	735.00	2.70	6.60	0.00	0.00
27.64	649.00	648.00	628.00	648.00	717.00	0.90	-0.30	0.00	29.93
27.70	602.00	601.00	613.00	602.00	717.00	0.80	-0.60	0.00	39.00
27.74	599.00	598.00	600.00	598.00	717.00	0.80	-0.50	19.30	39.70
27.77	593.00	593.00	591.00	593.00	717.00	0.80	-0.60	19.10	40.63
27.80	589.00	588.00	586.00	590.00	717.00	0.70	-0.50	18.90	41.42
28.00	842.00	842.00	803.00	833.00	756.00	2.20	0.80	0.00	0.00
32.39	752.00	751.00	689.00	751.00	709.00	1.10	-0.30	0.00	0.00
32.62	846.00	845.00	758.00	841.00	730.00	2.10	0.70	0.00	0.00
43.87	706.00	706.00	604.00	703.00	688.00	-0.30	0.30	0.00	41.42
44.61	600.00	600.00	606.00	600.00	687.00	-0.70	-0.30	0.00	55.62
44.64	596.00	585.00	606.00	596.00	687.00	1.00	-0.40	19.70	56.56
44.68	592.00	591.00	606.00	592.00	687.00	-0.50	-0.40	19.60	57.42
44.71	587.00	587.00	606.00	587.00	687.00	-0.60	-0.50	19.30	58.16
44.74	584.00	583.00	606.00	584.00	687.00	-0.60	-0.40	19.00	59.01

RESULTS OF HYDRATE RUN

TIME (HR)	PBAR (PSIA)	TBAR (DEG.C)	QBAR (CC/MIN)	CONV (%)	TIME	GMOL0	GMOLG	GMOLIN	GMOLOUT	GMOLN	CONV
0.000	748.000	-1.400	0.000	0.000	0.0000	4.8559	4.8559	0.0000	0.0000	0.0000	0.0000
0.033	722.000	-1.100	523.462	1.337	0.0330	4.8072	4.7143	0.0224	0.0710	0.0929	1.3365
0.066	718.500	-1.050	321.395	1.358	0.0660	4.7944	4.6584	0.0223	0.0351	0.1360	1.9578
0.099	711.500	-0.750	356.234	2.406	0.0990	4.7751	4.6079	0.0221	0.0414	0.1672	2.4064
0.132	705.500	-0.650	278.055	2.913	0.1320	4.7698	4.5674	0.0221	0.0275	0.2024	2.9129
0.232	768.500	-0.600	0.000	2.913	0.2320	5.1767	4.9743	0.4069	0.0000	0.2024	2.9129
4.013	607.000	0.000	0.000	18.082	4.0150	5.1767	3.9203	0.0000	0.0000	1.2564	18.0815
4.048	601.500	-0.150	325.162	18.436	4.0480	5.1679	3.8869	0.0246	0.0334	1.2810	18.4358
4.081	598.500	-0.050	310.947	18.645	4.0810	5.1617	3.8661	0.0246	0.0309	1.2956	18.6454
4.115	593.500	-0.200	308.578	18.996	4.1150	5.1559	3.8360	0.0246	0.0304	1.3199	18.9963
4.150	589.000	-0.300	370.871	19.155	4.1500	5.1392	3.8083	0.0248	0.0414	1.3309	19.1547
4.210	721.500	-1.350	0.000	19.155	4.2100	6.0139	4.6830	0.8747	0.0000	1.3309	19.1547
7.410	602.000	-0.250	0.000	30.544	7.4100	6.0139	3.8916	0.0000	0.0000	2.1223	30.5440
7.450	596.000	-0.150	507.290	30.357	7.4500	5.9607	3.8514	0.0187	0.0719	2.1093	30.3565
7.483	590.000	0.000	325.162	30.818	7.4830	5.9519	3.8105	0.0246	0.0334	2.1414	30.8184
7.545	583.000	-0.100	315.963	31.336	7.5450	5.9441	3.7667	0.0243	0.0321	2.1773	31.3358
7.580	579.500	-0.050	266.213	31.686	7.5800	5.9451	3.7434	0.0243	0.0233	2.2016	31.6856
7.795	887.000	-0.400	0.000	31.686	7.7950	7.9388	5.7371	1.9937	0.0000	2.2016	31.6856
16.630	693.500	0.550	0.000	49.922	16.6300	7.9388	4.4700	0.0000	0.0000	3.4688	49.9218
17.050	592.000	0.550	0.000	51.542	17.0500	7.3971	3.8158	0.0000	0.5417	3.5813	51.5415
17.083	587.000	0.850	353.590	51.866	17.0830	7.3832	3.7794	0.0246	0.0385	3.6038	51.8657
17.120	583.000	0.800	342.720	52.048	17.1200	7.3708	3.7543	0.0244	0.0368	3.6165	52.0480
17.149	580.000	0.950	300.077	52.286	17.1490	7.3660	3.7330	0.0244	0.0292	3.6331	52.2864
17.249	752.500	1.550	0.000	52.286	17.2490	8.4657	4.8326	1.0997	0.0000	3.6331	52.2864
19.749	700.500	1.000	0.000	56.963	19.7490	8.4657	4.5077	0.0000	0.0000	3.9580	56.9627
23.320	607.000	2.150	0.000	65.857	23.3200	8.4657	3.8897	0.0000	0.0000	4.5760	65.8566
23.353	599.000	3.850	404.734	66.610	23.3530	8.4432	3.8149	0.0249	0.0474	4.6283	66.6099
23.386	593.500	3.750	316.382	66.994	23.3860	8.4363	3.7812	0.0248	0.0317	4.6550	66.9943
23.420	588.500	3.700	283.216	67.428	23.4200	8.4352	3.7501	0.0248	0.0258	4.6852	67.4280
23.452	583.500	3.900	339.376	67.762	23.4520	8.4239	3.7155	0.0246	0.0359	4.7084	67.7624
23.636	750.000	5.150	0.000	67.762	23.6360	9.4627	4.7543	1.0388	0.0000	4.7084	67.7624
27.636	648.500	0.800	0.000	76.083	27.6360	9.4627	4.1761	0.0000	0.0000	5.2865	76.0828
27.703	601.500	0.600	0.000	74.878	27.7030	9.0792	3.8763	0.0000	0.3835	5.2029	74.8783
27.736	598.500	0.650	300.355	75.086	27.7360	9.0736	3.8563	0.0260	0.0296	5.2173	75.0862
27.770	593.000	0.600	353.449	75.362	27.7700	9.0580	3.8215	0.0238	0.0393	5.2365	75.3622
27.803	588.500	0.600	318.889	75.637	27.8030	9.0481	3.7925	0.0235	0.0334	5.2556	75.6372
28.000	842.000	2.000	0.000	75.637	28.0000	10.6541	5.3986	1.6060	0.0000	5.2556	75.6372
32.390	751.500	0.900	0.000	83.710	32.3900	10.6541	4.8377	0.0000	0.0000	5.8165	83.7097
32.620	845.500	1.900	0.000	83.710	32.6200	11.2395	5.4230	0.5853	0.0000	5.8165	83.7097
43.870	706.000	0.500	0.000	96.253	43.8700	11.2395	4.5514	0.0000	0.0000	6.6881	96.2532
44.607	600.000	0.000	0.000	97.344	44.6070	10.6390	3.8751	0.0000	0.6005	6.7639	97.3443
44.643	590.500	0.800	360.000	98.168	44.6430	10.6238	3.8026	0.0245	0.0397	6.8211	98.1683
44.676	591.500	0.050	340.351	97.753	44.6760	10.6118	3.8195	0.0244	0.0364	6.7923	97.7527
44.710	587.000	-0.050	309.831	98.046	44.7100	10.6045	3.7919	0.0240	0.0313	6.8127	98.0462
44.743	583.500	0.000	333.800	98.204	44.7430	10.5922	3.7686	0.0236	0.0359	6.8236	98.2044

METHANE HYDRATE FORMATION RUN # 5
 DATE RUN STARTED: 11-8-1987
 DATE RUN ENDED: 11-10-1987
 GRAMS OF H₂O= 907.900
 GRAMS OF SAND= 920.200
 HEIGHT OF THE CORE= 29.84CM.
 ROOM TEMPERATURE= 21.0000DEG.C
 TEMP.OF GAS LEAVING WET TEST METER= 16.7000DEG.C
 BAROMETRIC PRESSURE= 744.600MM.HG
 VAP.PRESSURE OF WATER AT TWTH= 14.100MM.HG
 ICE TO SAND VOL.RATIO= 2.787
 ICE TO SAND MASS RATIO= 0.987
 PERCENTAGE VOIDS IN THE CORE= 44.388
 GMOL.METHANE FOR 100 PERCENT CONVERSION= 8.764191
 HYDRATE FORMATION RUN INPUT DATA

TIME (HR.)	P1 (PSIA)	P3 (PSIA)	PL (PSIA)	PH (PSIA)	PR (PSIA)	T1RTD (DEG.C)	T2RTD (DEG.C)	FIREAD	VVTM (LIT.)
0.00	634.00	632.00	629.00	630.00	633.00	-1.90	-1.10	0.00	0.00
0.15	614.00	614.00	620.00	611.00	613.00	-1.00	-0.50	0.00	1.89
0.18	580.00	580.00	582.00	574.00	576.00	-0.80	-0.50	20.40	3.55
0.22	560.00	560.00	565.00	550.00	560.00	-0.80	-0.30	19.70	4.76
0.25	546.00	544.00	550.00	542.00	544.00	-0.90	-0.30	18.60	5.47
0.28	532.00	530.00	537.00	540.00	531.00	-0.90	-0.10	18.40	6.25
0.40	878.00	877.00	885.00	858.00	877.00	-0.90	-0.30	0.00	0.00
1.32	654.00	653.00	582.00	564.00	614.00	-0.80	0.00	0.00	6.25
2.40	594.00	583.00	654.00	582.00	564.00	-0.70	0.10	19.70	8.46
2.43	582.00	581.00	654.00	582.00	564.00	-0.70	0.00	20.00	9.43
2.47	571.00	571.00	654.00	582.00	564.00	-0.70	0.10	18.60	10.23
2.50	564.00	563.00	654.00	582.00	564.00	-0.70	0.20	18.70	11.12
2.72	841.00	840.00	770.00	581.00	563.00	-0.80	-0.10	0.00	0.00
4.71	706.00	705.00	693.00	569.00	563.00	-0.60	0.30	0.00	11.12
4.79	610.00	609.00	679.00	569.00	563.00	-0.60	0.10	0.00	29.00
4.82	602.00	602.00	657.00	569.00	563.00	-0.60	0.20	20.60	30.50
4.85	593.00	593.00	644.00	568.00	563.00	-0.50	0.20	20.10	31.49
4.89	588.00	587.00	642.00	569.00	563.00	-0.50	0.20	19.30	32.51
4.92	583.00	583.00	640.00	569.00	563.00	-0.60	0.10	19.50	33.38
3.22	868.00	859.00	827.00	568.00	563.00	-0.70	0.20	0.00	0.00
11.97	617.00	615.00	599.00	565.00	562.00	-0.60	0.40	0.00	0.00
13.22	590.00	590.00	564.00	565.00	561.00	-0.60	0.40	0.00	33.38
13.25	582.00	582.00	564.00	565.00	561.00	-0.60	0.50	19.70	34.80
13.29	576.00	576.00	560.00	565.00	562.00	-0.60	0.70	19.70	35.06
13.39	571.00	570.00	557.00	565.00	562.00	-0.50	0.70	19.60	36.46
13.45	567.00	567.00	552.00	565.00	562.00	-0.40	0.70	19.40	37.31
13.55	840.00	839.00	789.00	565.00	562.00	-0.70	-0.40	0.00	0.00
16.65	792.00	790.00	735.00	565.00	562.00	-0.80	0.50	0.00	0.00
19.40	742.00	740.00	670.00	561.00	561.00	-0.60	0.70	0.00	0.00
26.63	649.00	648.00	547.00	563.00	561.00	-0.60	0.80	0.00	37.31
26.79	607.00	606.00	544.00	563.00	561.00	-0.60	0.80	0.00	42.15
26.82	604.00	603.00	537.00	563.00	561.00	-0.50	0.90	19.50	42.91
26.85	598.00	598.00	534.00	563.00	561.00	-0.70	0.90	20.30	43.72
26.89	593.00	592.00	532.00	563.00	561.00	-0.50	0.90	19.50	44.54
26.92	589.00	588.00	529.00	563.00	561.00	-0.50	0.90	19.40	45.30
27.42	857.00	857.00	737.00	563.00	859.00	-0.70	1.00	0.00	0.00
37.17	767.00	766.00	609.00	763.00	769.00	-0.60	0.70	0.00	0.00
40.17	715.00	685.00	563.00	561.00	713.00	-0.70	-0.50	0.00	0.00
47.07	654.00	654.00	525.00	647.00	653.00	-0.70	0.20	0.00	45.30
47.14	602.00	602.00	525.00	608.00	610.00	-0.70	0.10	0.00	50.35
47.17	598.00	597.00	525.00	598.00	601.00	-0.70	0.30	19.80	51.66
47.23	589.00	588.00	525.00	589.00	593.00	-0.60	0.30	19.60	52.71
47.24	583.00	582.00	525.00	585.00	589.00	-0.70	0.40	19.60	53.59
47.27	579.00	578.00	525.00	579.00	584.00	-0.70	0.30	19.50	54.36

RESULTS OF HYDRATE RUN

TIME (HR)	PBAR (PSIA)	TBAR (DEG.C)	QBAR (CC/MIN)	CONV (%)	TIME	GMDLO	GMDLG	GMOLIN	GMLOUT	GMOLR	CONV
0.000	633.000	-1.000	0.000	0.000	0.0000	3.5603	3.5603	0.0000	0.0000	0.0000	0.0000
0.150	614.000	-0.250	0.000	0.416	0.1503	3.4804	3.4440	0.0000	0.0799	0.0365	0.4161
0.183	580.000	-0.150	535.276	2.095	0.1833	3.4356	3.2521	0.0254	0.0702	0.1836	2.0947
0.216	560.000	-0.050	423.837	3.083	0.2163	3.4090	3.1388	0.0245	0.0511	0.2702	3.0835
0.249	545.000	-0.100	297.770	3.958	0.2493	3.4021	3.0552	0.0231	0.0300	0.3469	3.9580
0.282	531.000	0.000	312.952	4.751	0.2823	3.3921	2.9757	0.0229	0.0330	0.4164	4.7510
0.315	877.500	-0.100	0.000	4.751	0.3990	5.3356	4.9192	1.9436	0.0000	0.4164	4.7510
1.316	653.500	0.100	0.000	19.110	1.3160	5.3356	3.6608	0.0000	0.0000	1.6748	19.1096
2.399	588.500	0.200	660.637	22.492	2.3990	5.2667	3.2955	0.0245	0.0934	1.9712	22.4918
2.432	581.500	0.150	369.096	22.748	2.4320	5.2506	3.2569	0.0249	0.0410	1.9937	22.7484
2.465	571.000	0.200	319.082	23.304	2.4650	5.2399	3.1975	0.0231	0.0338	2.0424	23.3043
2.498	563.500	0.250	341.091	23.626	2.4980	5.2256	3.1549	0.0233	0.0376	2.0707	23.6263
2.715	840.500	0.050	0.000	23.626	2.7150	6.7799	4.7092	1.5543	0.0000	2.0707	23.6263
4.715	705.500	0.350	0.000	32.306	4.7150	6.7799	3.9485	0.0000	0.0000	2.8314	32.3062
4.788	609.500	0.250	0.000	29.800	4.7880	6.0241	3.4125	0.0000	0.7557	2.6117	29.7995
4.821	602.000	0.300	498.782	29.855	4.8210	5.9864	3.3699	0.0256	0.0634	2.6165	29.8547
4.854	593.000	0.350	374.529	30.244	4.8540	5.9695	3.3189	0.0250	0.0418	2.6507	30.2443
4.887	587.500	0.350	376.057	30.378	4.8870	5.9504	3.2881	0.0240	0.0431	2.6624	30.3776
4.920	583.000	0.250	341.931	30.509	4.9200	5.9379	3.2641	0.0243	0.0368	2.6738	30.5086
5.220	863.500	0.250	0.000	30.509	3.2200	7.5084	4.8345	1.5705	0.0000	2.6738	30.5086
11.970	616.000	0.400	0.000	46.341	11.9700	7.5084	3.4470	0.0000	0.0000	4.0614	46.3411
13.220	590.000	0.400	0.000	48.001	13.2200	7.5084	3.3015	0.0000	0.0000	4.2069	48.0011
13.253	582.000	0.450	473.565	48.114	13.2530	7.6729	3.2561	0.0245	0.0600	4.2168	48.1135
13.286	576.000	0.550	198.877	48.664	13.2860	7.4864	3.2214	0.0245	0.0110	4.2650	48.6642
13.319	570.500	0.600	468.132	48.625	13.3910	7.4516	3.1900	0.0244	0.0592	4.2616	48.6249
13.352	567.000	0.650	336.498	48.720	13.3520	7.6398	3.1699	0.0241	0.0359	4.2699	48.7203
13.352	839.500	-0.050	0.000	48.720	13.5520	8.9753	4.7053	1.5355	0.0000	4.2699	48.7203
16.652	.791.000	0.350	0.000	51.896	16.6520	8.9753	4.4270	0.0000	0.0000	4.5483	51.8960
19.402	741.000	0.550	0.000	55.123	19.4020	8.9753	4.1442	0.0000	0.0000	4.8311	55.1235
26.625	648.500	0.600	0.000	61.034	26.6250	8.9753	3.6262	0.0000	0.0000	5.3491	61.0337
26.785	606.500	0.600	0.000	61.379	26.7850	8.7707	3.3913	0.0000	0.2046	5.3794	61.3792
26.820	603.500	0.700	315.883	61.495	26.8200	8.7628	3.3733	0.0243	0.0321	5.3895	61.4949
26.853	598.000	0.600	333.299	61.729	26.8530	8.7539	3.3438	0.0253	0.0342	5.4101	61.7293
26.887	592.500	0.700	330.091	61.975	26.8870	8.7435	3.3118	0.0243	0.0347	5.4316	61.9753
26.920	588.500	0.700	315.186	62.139	26.9200	8.7355	3.2895	0.0241	0.0321	5.4460	62.1393
27.420	857.000	0.650	0.000	62.139	27.4200	10.2372	4.7911	1.5017	0.0000	5.4460	62.1393
37.170	766.500	0.350	0.000	67.894	37.1700	10.2372	4.2868	0.0000	0.0000	5.9504	67.8944
40.170	700.000	-0.100	0.000	72.032	40.1700	10.2372	3.9242	0.0000	0.0000	6.3130	72.0316
47.070	654.000	0.250	0.000	75.027	47.0700	10.2372	3.6616	0.0000	0.0000	6.5756	75.0275
47.140	602.000	0.200	0.000	75.907	47.1400	10.0237	3.3711	0.0000	0.2134	6.6526	75.9069
47.173	597.500	0.300	448.214	75.858	47.1730	9.9930	3.3447	0.0246	0.0554	6.6483	75.9577
47.230	588.500	0.350	385.252	76.211	47.2300	9.9730	3.2937	0.0244	0.0444	6.6793	76.2112
47.240	582.500	0.350	344.996	76.448	47.2400	9.9602	3.2601	0.0244	0.0372	6.7001	76.4482
47.273	578.500	0.300	318.251	76.602	47.2730	9.9519	3.2383	0.0243	0.0325	6.7136	76.6023